# NUMERICAL INVESTIGATION OF SPORADIC-E LAYER FORMATION IN MIDLATITUDE

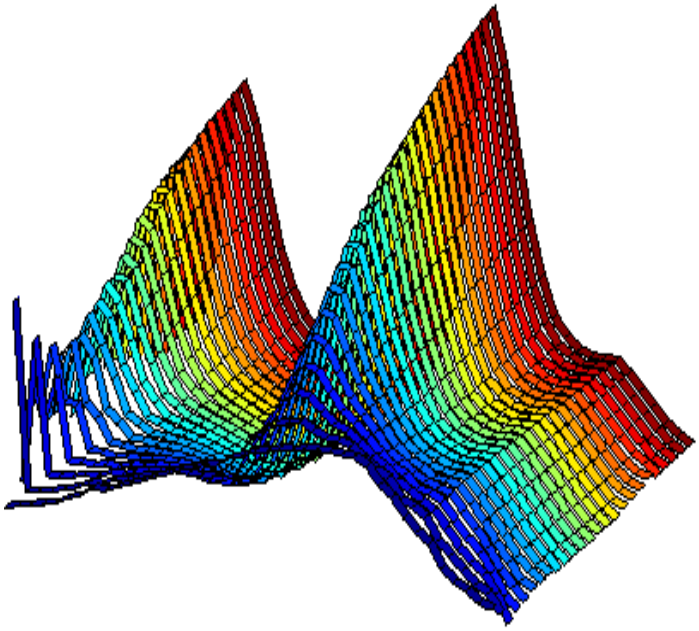

By

**Kibrom Bayru**

**Department of Physics,**
**Addis Ababa University**
**Ethiopia**

# NUMERICAL INVESTIGATION OF SPORADIC-E LAYER FORMATION IN MIDLATITUDE

by

**Kibrom Bayru**

**A thesis submitted to Addis Ababa University**
**Faculty Of Science Department Of Physics**

**In Partial Fulfillment of the Requirements for the Degree of**
**Master of Science in Physics**

# NUMERICAL INVESTIGATION OF SPORADIC-E LAYER FORMATION IN MIDLATITUDE

Dr. Baylie Damtie, Advisor

Examiner:

Dr. A.K Chaubey, Committee Chair

Dr. Esayas Belay, Examiner

Dr. Gizaw Mengistu, Examiner

Date Approved

**I dedicate this work to:**

**Bayru Kiros**

**Alganesh Yayine**

**Aster Yayine**

**Gennet Yayine**

# PREFACE

No matter how we evolve in our educational choice, it is good to let others know that one at least can drive it to his closest point of interest. When you involve yourself in the rhythm of scientific and technological advancement you face a lot of problems and challenges, nature being the cause of almost all of the challenges.

Being involved in the rhythm, not only did I get a kick of pleasure, but also I felt responsible to convey my aspect of tackling the challenge. Having your scientific challenge put yourself at the center of concentric circles of radius extending to infinity. you are at the center, assuming you know almost nothing. And the nearest rims of circles representing explorations by other people. Now you have two obligations one is: it is a must that you reach the nearest final rim for you to catch up. Two is you must fight to swim at least beyond the final rim at hand for you to discover. It is oblivious that that you cannot swim to the radius at infinity, due to limit of age and limitlessness of knowledge. Bearing this in mind you can start your problem.

To clearly grab the core concept of the problem, we have tried to categorize the content of this thesis into chapters. Chapter one introduces the problem with a little historical background of theoretical formulation. Chapter two tries to explain the background information needed to develop the problem, and the theoretical formulation to understand the problem. Chapter three deals with characterizing the problem on the basis of experimental observation. Chapter four is all about numerical investigation of the problem on the basis of theoretical formulation and observation.

Kibrom Bayru
Addis Ababa University

# ACKNOWLEDGEMENTS

Behind this thesis stand a whole bunch of people who supported me to achieve an end point. Enumerating them in relevance to their help would be very hard or be part of the thesis which needs a thorough investigation. But at least it is possible to divide them into groups, which include professional supporters, friends, and families.

Out of the professional supporters, my first thanks goes to Dr. Baylie Damtie, who chose me a fascinating probelm and helped me develop insights of it. In my evolution of understanding the tweaks and tricks of the problem, a bigger share goes to DR. Esayas shumme, which I am very grateful of. After developing the problem a challenge occurred in finding suitable data, which was later completely peeled off by the support of Barbara Emery from CEDAR data base and Dr. Patrick A. Roddy from Texas University. A facility to stay in Bahir-Dar under close supervision of my advisor was set by the department of physics, which I am very thankful.

Friends who contribute greatly to this work are listed below fearing that it will not put me in quarrels with unmentioned friends. My partners Antenehe and Tadesse, who were involved in similar thesis problems, which are some how related to mine helped me understand the problem better. Some of the friends who have been guarding me from any obstacle related to this work are Aron kassahun, Mohammed-seid Nuru, Yohannes Fekre, Habtom G/micheal, Senait Mekonnen, Feven Busa, Ermias Yehdego, Seged Kelmu and Melaku.

From family supports, my humble respects goes to my father. Not only did my father consistently helped me financially, but also he was very enthusiastic in my field of study, which gave me this inner energy to hold up. Next dearest respect goes to my mother who got this big ears to listen to what ever I have to say, and put me in the finest peace of mind. I would dare say that she was my personal manager all the way up here. It would be very hard to say that I alone without my seven sisters and a brother could survive any challenges in life. Best of all my sister Saba was fulfilling accessaries I needed in developing my thesis. My second moms Aster and Genni were always by my side in perusing my education. It is very hard to mention all the people who supported me, and

this is a fraction of them, and finally I have to say I am very grateful for all the people who have supported me.

Kibrom Bayru

# TABLE OF CONTENTS

# LIST OF TABLES

# LIST OF FIGURES

# ABSTRACT

In this thesis numerical investigation of wind shear theory, which is responsible for the formation of sporadic-E layers in midlatitude is presented. Numerical investigation of sporadic-E layers were pursued since the late 1960s. However, numerical modelling efforts were limited due to lake of input parameters. A recent rocket observation from Wallops Island Flight Facility (WIFF), VA (37.84 N, 75.48 W) of sporadic-E layers is used in this investigation. In this observation secondary peaks other than sporadic-E layers were observed unlike previous campaigns, which could question the validity of wind shear theory. Numerical investigation confirms that tidal winds are responsible for the formation of dense ion layers in the 90-130km height region. It is demonstrated that the assumed sources of transport mechanisms actually form E-region layer densities similar to those observed. The numerical investigation also shows that zonal and meridional winds and electric fields each play distinct roles in local transport and formation of secondary peaks.

# CHAPTER 1

# INTRODUCTION

Plasma enhancements above the normal background ionization that have relatively narrow altitude and broad horizontal extent in the lower E-region of the ionosphere are called sporadic-E layers. The horizontal extent of sporadic-E layer varies from tens to hundreds of kilometers and it is usually situated in altitudinal range of 100-110km. The peak plasma density is about an order of magnitude larger than the ambient plasma density. Though the nature of the phenomena is highly dependent on the nature of instruction used to observe it [Mathew 1997], the phenomena sporadic-E observed in ionosonde records has been well established to be associated with thin layers of enhanced ionization. Taking this into account a review on observation of sporadic-E layers is included in this thesis.

Rocket study of these layers confirm that the enhanced ionization are abundant in metallic ions, which are deposited in the ionosphere by meteor ablation [Roddy 2004]. Metallic ions have long life time for recombination can therefore accumulate in thin layers under certain circumstances under the action of neutral winds and electric fields.

Dungey (1956) suggested that the layers can be produced by the action of wind shear. This theory was later fully developed by Whitehead (1961) and Axford (1963), and it states that the layer will be formed at altitudes where the ion vertical velocity has a convergent null, that is an altitude where the velocity is zero and flow is upward from below and down from above. Horizontal neutral wind shear associated tides and gravity waves can drive the ions against the Earth's magnetic field can create such situation. Detailed mathematical clarification and numerical investigation of wind shear theory is included in later sections as it is the core of this thesis.

The purpose of this thesis is two fold. First we shall carefully investigate sporadic-E layers observation. We then go on to refine our understanding of sporadic-E layers by systematically studying wind shear models and comparing them to the observations.

But before directly coming to the purposes of this paper a brief overview of study area and background of the phenomena will be discussed in Chapter two. Sporadic-E layers being an ionospheric phenomena and ionosphere being ononized part of the atmosphere

a general introduction and discussion will be the objective of this chapter.

Chapter 3 will be devoted to a thorough observational study of sporadic-E layers. An *in situ* measurement by rocket which was taken over Wallops Island is treated in this Chapter. The purpose of the experiment was to measure the time evolution of conditions related to sporadic-E layers and other sub-peaks. Simultaneous measurement of electron density profile, neutral wind profile, electric field profile, and relative composition of metallic and molecular ions within the layer was observed in the experiment.

The above measured parameters are very useful in the numerical investigation of the theory responsible for the formation of sporadic-E layers. Using the measured parameters Chapter 4 is devoted to numerical investigation of the theory and to study its consistency with observation.

# CHAPTER 2

# BACKGROUND INFORMATION AND THEORY

## 2.1 The Atmosphere of the Earth

The atmosphere of the Earth is gas suspension engulfing the earth, its origin and bulk composition being traced to release of gases from the surface ($N_2, H_2O, CO_2$), nuclear radioactive decay ($Ar, He$), and biophotosynthesis ($O_2$) over the past billion years.

The atmosphere is a mixture of neutral, ionized and electron gases that have coupled chemistry and dynamics. The study of the upper atmosphere is incomplete without the inclusion of all of these species. The altitude above which ions exist in significant numbers is known as the ionosphere. The presence of charged particles is a result of ionizing solar radiation incident on the denser neutral gas of the upper atmosphere. We begin this introductory chapter with a review of the neutral atmosphere's structure. This is followed by an introduction to the formation and chemistry of the ionosphere and in particular, the E-region and the role of metallic ions.

### 2.1.1 Temperature Regions

The atmosphere can classified into spheres with height using a parameter of our choice. Commonly used stratifying parameters are temperature, number density, composition, and molecular mass. The atmosphere is most often subdivided by vertical gradients in temperature into layers termed as troposphere, stratosphere, mesosphere, and thermosphere see Figure 1. The boundaries between each spheres are called pauses.

The lowest sphere in this arrangement, the troposphere, extends from the ground up to the tropopause at $\sim 10km$ altitude and is characterized by a negative temperature gradient with increasing altitude. The main heat source for the troposphere is the solar heating near the Earth's surface. The next layer, the stratosphere, extends from the tropopause up to the stratopause at $\sim 50km$ and is characterized by a positive temperature gradient with increasing altitude. The heat source at $\sim 50km$ altitude is due to the absorption of solar ultra-violet radiation by ozone. The mesosphere extends from the

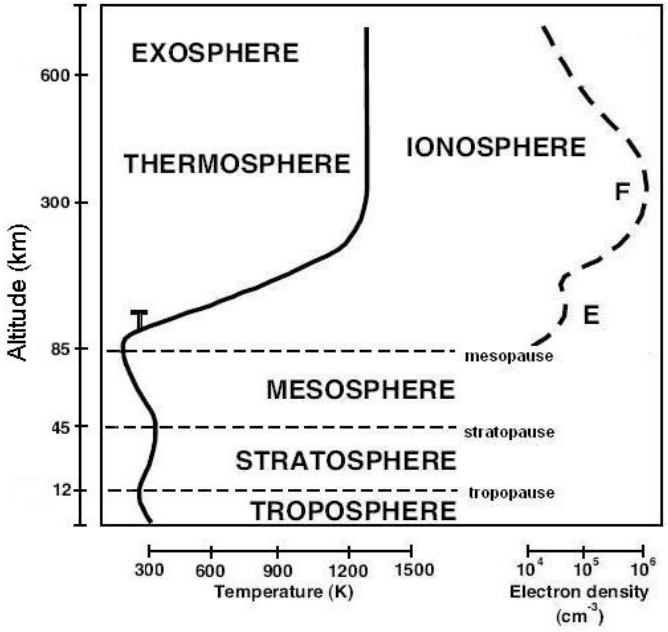


Figure 1: The solid and broken vertical lines indicate the variation of temperature and electron density with altitude, respectively [Agabi 2004].

stratopause out to the mesopause at $\sim 80km$ and is characterized by a negative temperature gradient with increasing altitude. The thermosphere/exosphere composes the whole of the remaining atmosphere above the mesopause. Temperature distribution (>1000 K) of the thermosphere is due to the absorption of solar ultraviolet/extreme ultraviolet rays.

### 2.1.2 Barometric Distribution

A fundamental property of the neutral atmosphere is that its pressure and density decrease with increasing altitude in accordance with expectations from hydrostatic equilibrium. Gases are compressible and the gas at any given altitude is compressed by the weight of the gas above it. Since the amount of gas weighing down on an element volume of air at any given altitude decreases with increasing altitude, the pressure and density of the atmosphere fall off exponentially with increasing altitude. The rate of change of the atmospheric density with altitude can be described by

$$dp = -g\rho dz, \tag{1}$$

where $p$ is the neutral pressure, $g$ is the gravitational acceleration, $\rho$ is the neutral mass density, and $z$ the altitude. Using the ideal gas law, equation (1) can be expressed as

$$dp = -\frac{mg}{kT} p dz, \tag{2}$$

where $T$ is the temperature. Now let us introduce the relation

$$H = \frac{kT}{mg}, \tag{3}$$

where $H$ is the scale height, this parameter lumps the local gravitational and thermodynamical characteristics of a given atmospheric volume. From $mgH = kT$ we can relate $H$ to the height above $z$ where an air molecule has increased its gravitational potential energy by an amount of the order of its thermal kinetic energy at $z$.
Integrating equation (2) assuming $H$ to be constant with height (isothermal), we obtain

$$p = p_o \exp -[\frac{\Delta z}{H}], \tag{4}$$

where $p_0$ is the pressure at initial height and $\Delta z$ is the height from initial to height $p$ is calculated. The gas number density can also be expressed by

$$n = n_o \exp -[\frac{\Delta z}{H}], \tag{5}$$

where $n_0$ is the number density of the neutral gas at initial height and $n$ indicates the number density at $\Delta z$ height above the initial height.

What equation (5) shows is that the density of neutral gas in the atmosphere decays exponentially with increasing altitude. At a high enough altitude ($> 60$km) the density of neutrals becomes low enough that ions and free electrons can have an appreciable lifetime, thus allowing the formation of the ionosphere. Also, since the scale height in equation (3) is a function of mass, the rate of exponential decrease for different gases depends on their masses. This leads in part to a stratification of the composition of the neutral atmosphere visible in Figure 2. This variation in neutral composition strongly influences the ion composition and chemistry of the ionosphere.

## 2.2 The Ionosphere

Solar radiation incident upon rarefied gases in the upper atmosphere produces a region of significant ionization known as the ionosphere. The ionosphere covers an altitude

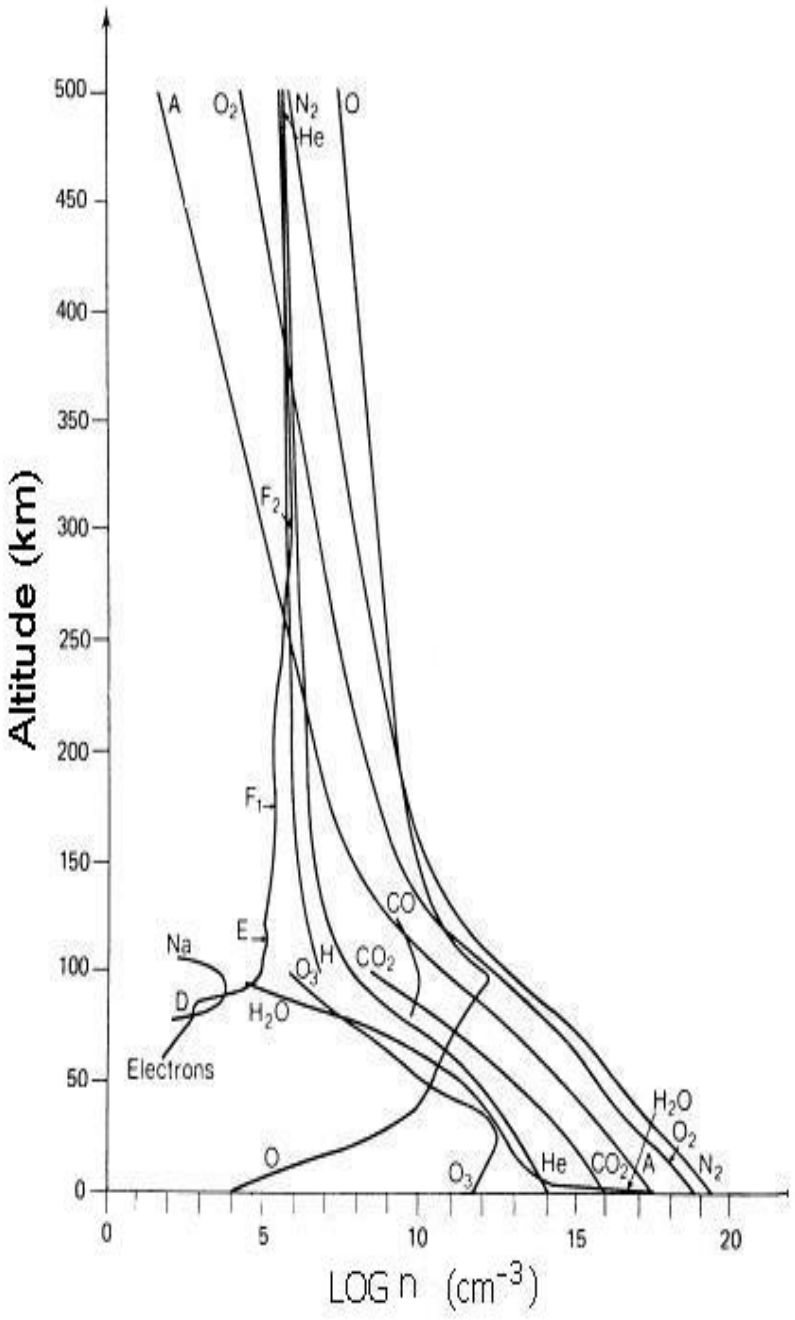


Figure 2: Altitude variation of atmospheric constituents [Roddy 2005].

range from ∼60 km to some thousands of kilometers. Distinct regions of ionization develop within the ionosphere primarily due to altitude variations in (a) intensity of solar radiation incident on a region, (b) the chemical composition and reactions within the region, and (c) the neutral density of the region (as discussed above). The first region of the ionosphere to be discovered was given the name E region to denote it as electrified region. The distinct regions above and below the E region were then called the F and D regions. The F region was later subdivided into F1 and F2. The following is a review of the fundamental processes responsible for the formation of these ionized regions.

### 2.2.1 Chapman Layers

Nearly all of the ionization in the upper atmosphere at midlatitude is due directly or indirectly to solar radiation. The ionization rate, $q$, at any altitude can be expressed by

$$q = \Lambda \sigma n_n I, \tag{6}$$

where $\Lambda$ is the ionization efficiency of the neutral species, $\sigma$ is the absorption coefficient of the neutral species for a specific frequency of radiation, $n_n$ is the neutral species number density, and $I$ is the intensity of the radiation. The neutral density was expressed in the previous section in equation (6), $\Lambda$ and $\sigma$ are experimentally determined quantities, so only the radiation intensity remains to be quantified. The spectrum and intensity of the radiation received at any altitude is dependent on the current solar activity and the effect the atmosphere above that altitude has had on that radiation. The rate at which the intensity of solar radiation is attenuated as it passes though the atmosphere can be expressed by

$$dI = -I\sigma n ds = I d\tau, \tag{7}$$

where $\tau$ is referred to as the optical depth, see Figure 3.
From equation (7), we can obtain

$$I = I_\infty \exp[-\sigma H n_o \exp[\frac{-z}{H}] \sec(\theta)], \tag{8}$$

where $I_\infty$ is the intensity of radiation at the top of the atmosphere, and $\theta$ is the solar zenith angle. Subsequently, the production rate, $q$ , can be written as

$$q = q_0 \exp[-z/H]. \exp[-n_0 H \sigma \sec(\theta) \exp[-z/H]], \tag{9}$$

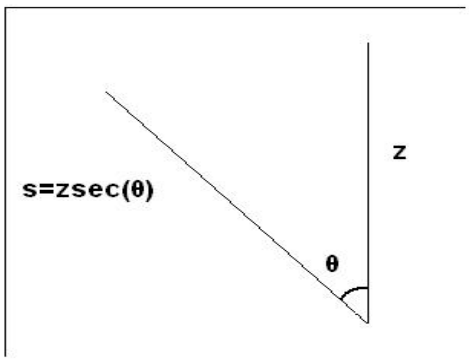


Figure 3: The slant path of solar radiation s.

where $q_0$ is the production rate at initial height and $q$ is the rate of production of ionization (production function) which is proportional to the rate at which ionization is absorbed by the neutral atmosphere constituents.

We see that the production rate is proportional to the product of an exponential and the exponential of an exponential. This function has a maximum at some z, so that there will be an altitude range, or layer, where the ionization rate is maximized.

The formation of a region of ionization by this mechanism was first treated by Sydney Chapman and is so referred to as a Chapman layer. To a great extent, the ionosphere can be thought of as a superposition of multiple Chapman layers with maxima at different altitudes, each based on different chemistry and ionizing radiation.

The degree of transmittance of the neutral atmosphere is a function of wavelength. The $F$ region ($> 200km$) is populated by $O^+$ ions ionized mainly by solar EUV ($15-80nm$) as shown in Figure 4. The $E$ region ($100 - 150km$) consists mainly of $O_2^+$ and $NO^+$ produced by soft x-rays and $80 - 100nm$ UV. There is more to be said on the E region in subsequent chapters. The D region is produced by the most penetrating solar radiation and has a very complex chemistry associated with the high neutral density. The ion density of all these regions is subject to variations in solar activity.

The $D$, $E$, and $F_1$ regions are Chapman type layers and therefore represent a balance between production and recombination loss. Consequently, when the main source of production diminishes at sunset the ionization within the regions rapidly decays. The very high neutral density and dominant number of molecular ions in the $D$ and $E$ regions

results in their very rapid disappearance after sunset due to dissociative recombination. Figure 5 illustrates day and night variation of ion densities. The day time ion density is sreduced in the night time due to recombination. Significant ionization layers do exist in the night time E region, and are treated as the major focus of this work.

## 2.3 The E-Region

The E-region ionosphere extends from around 100 to 160 km and is mainly populated by $O_2^+$ and $NO^+$ with lesser concentrations of $O^+$ and $N^+$ present during the day. Peak daytime electron densities reach about $10^5 cm^{-3}$ (105-110km) with nighttime values being an order of lower magnitude. Neutral species include significant concentrations ($10^{14} - 10^{10} cm^{-3}$) of $N_2$, $O_2$, and $O$ along with some $CO_2$. Daytime photo-ionization of $O_2$ by solar UV with $\lambda < 103nm$ is responsible for the majority of the ions either directly or indirectly through chemistry with neutral species. The basic E-region chemistry can be summarized as

$$O_2 + h\nu \longrightarrow O_2^+, \tag{10}$$

$$O_2^+ + N_2 \longrightarrow^{k_1} NO^+ + NO, \tag{11}$$

$$O_2^+ + NO \longrightarrow^{k_2} NO^+ + O_2. \tag{12}$$

Soft x-rays ($\lambda < 80nm$) also produce $N_2^+$ which then reacts quickly to form other ions in the following manner

$$N_2^+ + O_2 \longrightarrow^{k_3} O_2^+ + N_2, \tag{13}$$

$$N_2^+ + O \longrightarrow^{k_4} NO^+ + N, \tag{14}$$

where $k_{i=1,2,3...}$ s, are the rate coefficients of E-region chemistry.

Significant layers of metallic ions of meteoric origin may also be present in the E region. Numerical modelling of these metallic ion layers are the main goal of this thesis. Direct ionization of the E region effectively shuts off after dusk, so at night the region is dominated by recombination chemistry, transport, and meteoric input. The main ion loss mechanisms in the E region are due to dissociative recombination and this includes

$$NO^+ + e^- \longrightarrow^{k_5} N + O, and \tag{15}$$

$$O_2^+ + e^- \longrightarrow^{k_6} 2O. \tag{16}$$

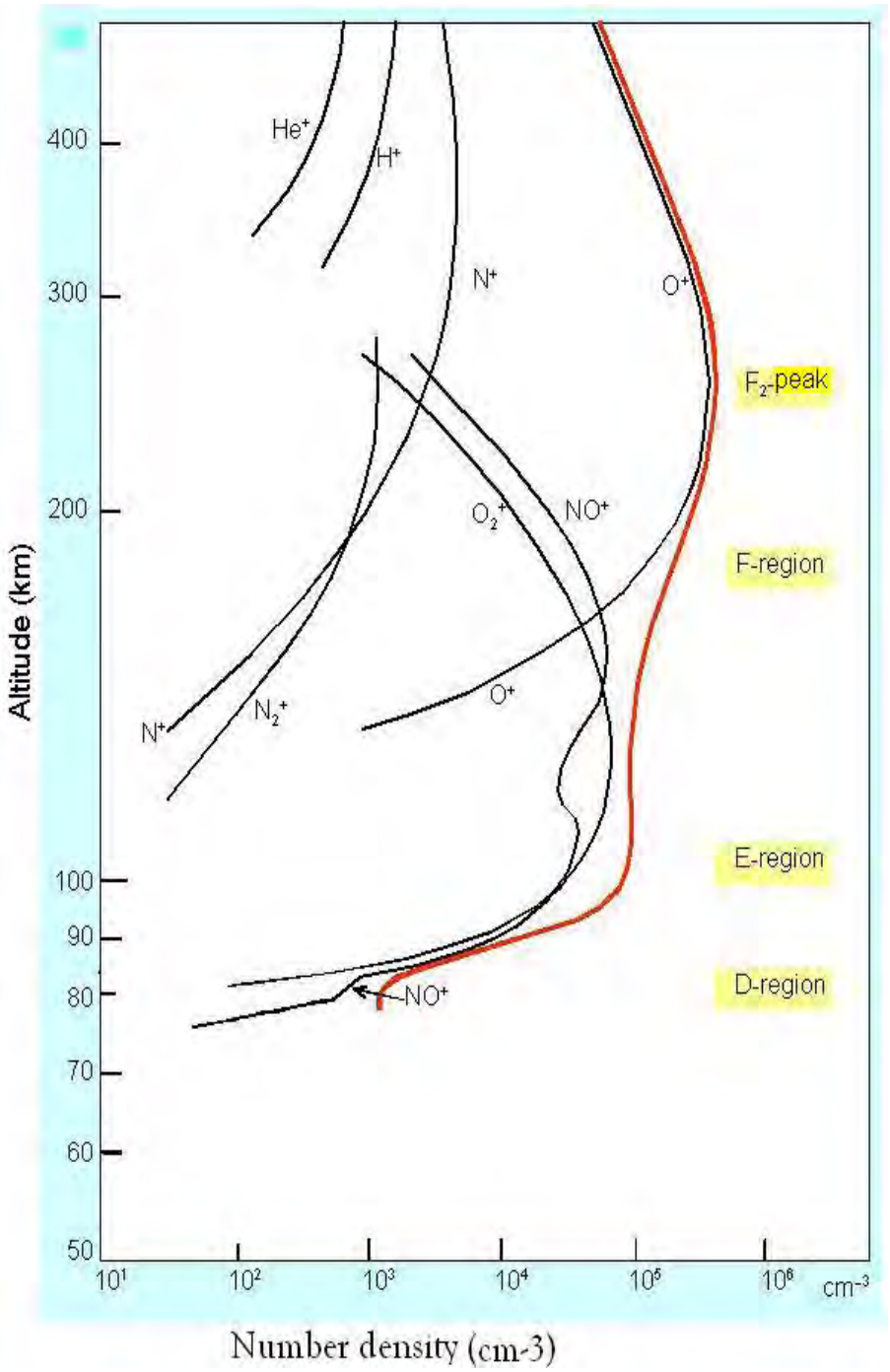


Figure 4: Ion composition and regions of the ionosphere [Radicella, lecture notes ICTP, 2000].

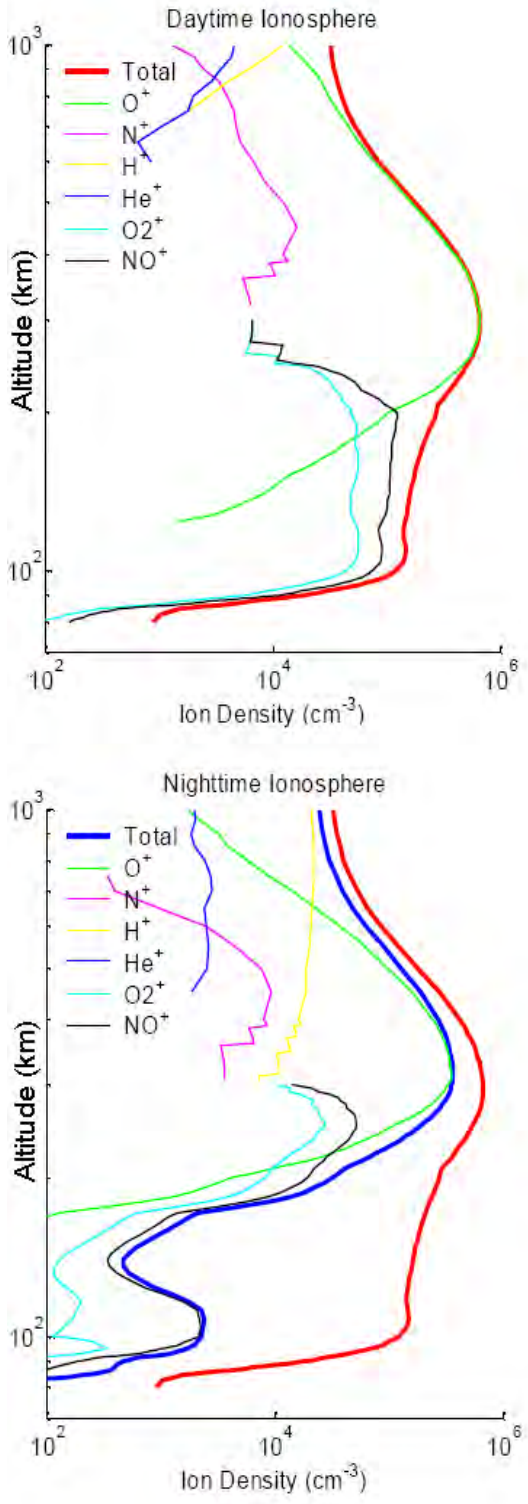


Figure 5: Day and night ion density profile from IRI-95 [Roddy 2005].

Table 1: Rate Coefficients for E region chemistry [Roddy 2005].

| $k_x$ | Rate Coefficients ($cm^3 s^{-1}$) | Source |
|---|---|---|
| $k_1$ | $2.0 \times 10^{-16}$ | Banks and Kockarts [1973] |
| $k_2$ | $4.0 \times 10^{-10}$ | Torr and Torr [1979] |
| $k_3$ | $1.5 \times 10^{-11} T_i = 800K$ | Torr and Torr [1979] |
| $k_4$ | $1.4 \times 10^{-10}(T_i/300)^{-0.44})$ $T_i < 1500K$ | Torr and Torr [1979] |
| $k_5$ | $4.2 \times 10^{-7}(T_e/300)^{-0.85})$ | Torr and Torr [1979] |
| $k_6$ | $2.1 \times 10^{-7}(T_e/300)^{0.55})$ | Torr and Torr [1979] |

$O_2^+$ is also effectively lost in the formation of $NO^+$ through the reactions shown in equations (11) and (12). There is therefore a persistent source of $NO^+$ in the E region after sunset but there is no corresponding source for $O_2^+$.

The equations above are only a fraction of the possible reactions, but they represent the primary reactions in the nighttime E region. The temperature dependent rate coefficients are difficult to quantify and consequently vary depending on the reference and technique used to determine them [Roddy 2005]. Table 1.1 lists the rate coefficients in their entirety. Because neutral species participate in reactions equations (12) and (13), ion neutral collisions need to be examined. The ion neutral collision frequency is defined as

$$\nu_{in} = N_n \sigma v_{th}, \tag{17}$$

where $N_n$ is the neutral density, $\sigma$ is the collision cross-section, and $v_{th}$ is the ion thermal velocity. $\nu_{in}$ is a function of both the neutral density and the ion temperature and is therefore a strong function of altitude. Collisions with neutrals are also fundamental to the formation of the plasma layers under study here.

## 2.4 Meteoric Species

On the order of $10^8 kg$ of extraterrestrial material is intercepted by the Earth each year [Carter and Forbes 1997]. That flux represents a tremendous amount of potentially ionizable material that can play a significant role in the ionosphere.

The two main sources for this material are cosmic dust and the meteoroids from the ablation and subsequent disassociation of asteroids and comets.Gravity accelerates the extraterrestrial material as it approaches the Earth until frictional heating with the atmosphere either vaporizes it completely or it strikes the surface. Most of this vaporization

of material takes place between 90 and 110 km as cited in [Alain 1978]. The ablated material can then be ionized by the heat of ablation, incident solar radiation, or charge exchange with ions.

Meteoric ions have been observed in the ionosphere by satellites, Lidar, and over 50 rocket-borne ion mass-spectrometers [Roddy 2004]. Meteoric ions in the form of $Na^+$, $Mg^+$, $Si^+$, $K^+$, $Ca^+$, $Fe^+$,$Si^+$ have all been detected (with $Fe^+$, $Mg^+$, and $Si^+$ the most prevalent) along with a host of metal compounds [Roddy 2005].

Metal ions in the nighttime E region are neutralized by either radiative recombination with electrons or by the formation of a molecular ion that is then neutralized by dissociative recombination [Ferguson 1972] cited with in [Roddy 2005]. The radiative recombination rate for atomic metal ions is roughly five orders of magnitude smaller than for most molecular ions under similar conditions. Metal ions can therefore persist for a long time (relative to molecular species) in dense layers without being neutralized. The increased electron density associated with a dense layer of metallic ions will also result in the increased dissociative recombination of molecular species.

## 2.5 Sporadic-E layers

A closer look upon the large scale D, E, and F region stratification of the ionosphere there may be finer transient structures that appear as plasma enhancements or depletions. Enhancements above the normal background ionization that have a relatively narrow altitudinal and broad horizontal extent can be called layers. Generally we find two type of these layers differentiated basically on their altitudinal occurrence. The first one is sporadic-E, which is observed in the lower part of E-region in the range of 100 to $110km$. The others are secondary peaks which are observed in the transitional valley region between E and F layers, in the range of 110 to 200km. Latitudinal variation of ionospheric characteristics affect the formation theory of these layers. In mid latitude the effect of winds driven by internal gravity waves or atmospheric tidal winds dominate the formation of the layers [Axford, 1963; Osterman et al., 1994; Bishop et al., 2005] as cited within [Roddy]. In high latitude the effect of existing electric field become responsible for the formation of these layers as compared to contribution of winds, [Bristow 1991]. Let us now describe the theory that is used to study sporadic-E layer in midlatitudes.

### 2.5.1 Wind Shear Theory

Sporadic E layers are caused by the redistribution of plasma through the interaction of the plasma embedded in the neutral atmosphere with the geomagnetic field under an appropriate vertical profile of the horizontal wind velocity. This mechanism is called the wind shear theory which was established by Whitehead (1961) and Axford (1963). The fact that appears basic to the wind shear theory of sporadic-E is the ratio of the ion-neutral collision frequency to the ion gyro-frequency is of the order of 1-10 with in the altitude range where neutral wind shears are high. Thus ions interact strongly with the neutrals through collisions and with geomagnetic filed through Lorentz force, while electrons interact with ions through plasma polarization field.

Considering now the macroscopic motion of heavy ions in the ionosphere under the influence collision and Lorentz force, the equation may then be written as

$$\frac{d\mathbf{v}_i}{dt} = \nu_{in}(\mathbf{u} - \mathbf{v}_i) + \frac{e}{m_i}(\mathbf{E} + \mathbf{v}_i \times \mathbf{B}), \tag{18}$$

where $e$, $m_i$, $\mathbf{v}_i$ are the charge, mass, drift velocity of the ions, $\mathbf{u}$ is the neutral gas velocity, $\mathbf{E}$ is the electric field and $\mathbf{B}$ is the local geomagnetic field (assumed homogenous over the region considered). The processes of interest is rather slow that is the length-scale of the processes is larger than the mean ion free path, and the time scale is larger than the inverse value of ion neutral collision frequency (the charged particles undergo many collisions with neutrals during the time of interest). Hence it is possible to neglect the so called inertia term that is $\frac{d\mathbf{v}_i}{dt} = 0$. The only electric field considered is that required to prevent charge separation (due to the electric field $\mathbf{E}$, electrons tend to follow ions, other background electric fields are ignored), then the electric field term can be ignored. Using the above assumptions ($\frac{d\mathbf{v}_i}{dt} = 0$ and$\mathbf{E} = 0$) equation (18) can be written as

$$\rho_i(\mathbf{u} - \mathbf{v}_i) + \mathbf{v}_i \times \mathbf{B} = 0, \tag{19}$$

Where

$$\mathbf{B} = B_0\hat{\Gamma}, \tag{20}$$

$\hat{\Gamma}$ is a unit vector in the direction of magnetic field and the ratio of collision frequency to the gyro-frequency is given by

$$\rho_i = \frac{\nu_{in}}{\Omega_i}, (\Omega_i = \frac{B_0 e}{m_i}). \tag{21}$$

Combining equations (19) (20) (21)

$$\mathbf{v}_i = \frac{1}{1+\rho_i^2}[\rho_i^2\mathbf{u} + \rho_i\mathbf{u}\times\hat{\Gamma} + (\mathbf{u}.\hat{\Gamma})\hat{\Gamma}]. \tag{22}$$

Equation (22) shows that the ion velocity has components parallel to the neutral wind, perpendicular to the geomagnetic field and the neutral wind, parallel to the geomagnetic field. The direction of the geomagnetic field may be taken as to be constant over the region of interest, but both $\rho_i$ and $\mathbf{u}$ vary with altitude, hence the magnitude and direction of the ion drift velocity vary with altitude. The variation is such that a net flow into some altitude is established, then a sporadic-E layer can form. The amount of the net flow of ionization into a region is measured by the convergence (the negative divergence) of the ion velocity field. It is the study of the variation of ion velocity field with altitude which is the focal point of wind shear theory. However it is also worthy studying other properties of ion drift velocity.

It is convenient to distinguish the three contributions to the ion drift velocity as follows

$$\mathbf{v}_i = \mathbf{v}_{ic} + \mathbf{v}_{im} + \mathbf{v}_{ig}, \tag{23}$$

where

$$\mathbf{v}_{ic} = \frac{\rho_i^2}{1+\rho_i^2}(\mathbf{u}), \tag{24}$$

$$\mathbf{v}_{im} = \frac{\rho_i}{1+\rho_i^2}(\mathbf{u}\times\hat{\Gamma}), \tag{25}$$

and

$$\mathbf{v}_{ig} = \frac{1}{1+\rho_i^2}(\mathbf{u}.\hat{\Gamma})\hat{\Gamma}. \tag{26}$$

In the lower E-region ($< 120$km) $\rho_i \gg 1$, and the drift velocity takes the approximate form

$$\mathbf{v}_i \simeq \mathbf{v}_{ic} \simeq \mathbf{u}, \tag{27}$$

since $\mathbf{v}_{im}$ and $\mathbf{v}_{ig}$ are of order of $\rho_i^{-1}$ and $\rho_i^{-2}$, respectively. At the lower altitudes the collision force dominates over the geomagnetic force and ions are carried along with the neutrals with their velocity. $\mathbf{v}_{ic}$ is seen to represent primarily the effect collisions on the

ion motion. The direction of this component is always the same as that of the neutral wind and it's magnitude

$$v_{ic} = \frac{\rho_i^2}{1+\rho_i^2}(u). \tag{28}$$

High in the E-region ($>$ 140km) $\rho_i \ll 1$, and the drift velocity becomes

$$\mathbf{v}_i \simeq \mathbf{v}_{ig} \simeq (\mathbf{u}.\hat{\Gamma})\hat{\Gamma}, \tag{29}$$

since $\mathbf{v}_{ic}$ and $\mathbf{v}_{im}$ are of the order of $\rho_i^{-2}$ and $\rho_i^{-1}$, respectively. At the higher altitudes the geomagnetic force predominates over the collision force and the ions are driven along the geomagnetic field lines by the neutral wind. The direction of this component is either parallel or antiparallel to the geomagnetic field lines and its magnitude is

$$v_i = \frac{1}{1+\rho_i^2} u\cos(k), \tag{30}$$

where $k$ is the angel between the neutral wind and the geomagnetic field.

At the intermediate altitudes ($<$ 130km) the ratio of collision to gyrofrequency is of order unity, i.e, $\rho_i = 1$, hence all three terms in the expression are important for the ion drift velocity. It is in this region that the effect of the second term in equation (23) is most felt. The direction of this component of the drift velocity is perpendicular to both the direction of the neutral wind and of the geomagnetic field, and its magnitude is

$$v_{im} = \frac{\rho_i}{1+\rho_i^2} u|\sin(k)|. \tag{31}$$

Ignoring the geometrical effect (the variation of), this component exhibits a maximum value at that altitude where $\rho_i = 1$. In this case, both collision and magnetic field are equally important. It vanishes where either effect dominates (either where $\rho_i \to 0$ or where $\rho_i \to \infty$, see Figure 6). The altitude region where this effect contributes appreciably to the ion drift motion (from 100 to 130km) is covered very nicely the altitude region where midlatitude sporadic-E layers are frequently observed.

### 2.5.2 Ion Drift Velocity Convergence

The tendency for a net flow of ions from a particular region to exist is measured by the divergence of the ion drift velocity. As it is apparent that from the form of the expression

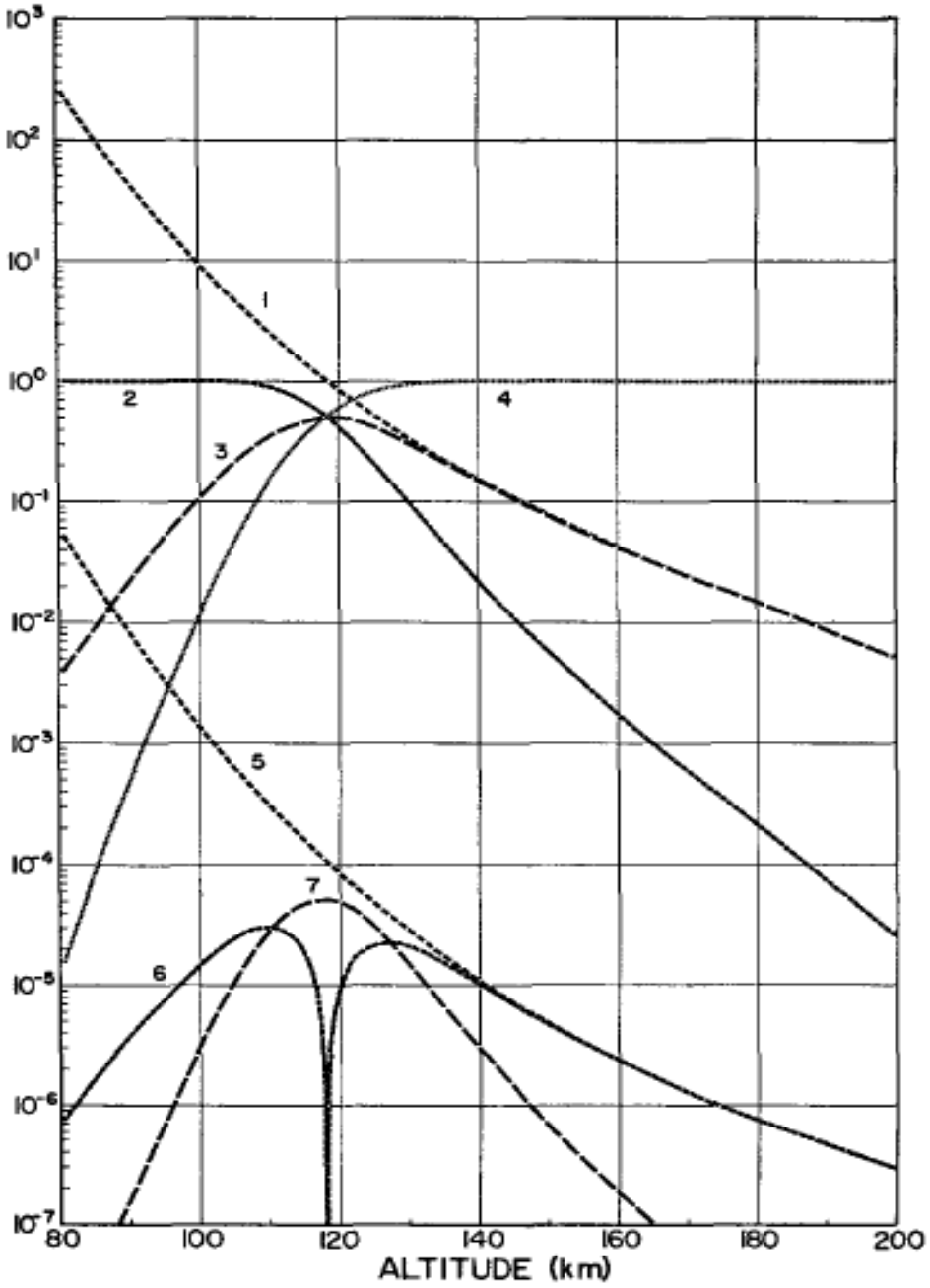


Figure 6: Altitude profile of collision frequency to gyrofrequency in different ratios. (1) $\rho_i$; (2) $\frac{\rho_i^2}{1+\rho_i^2}$; (3) $\frac{\rho_i}{1+\rho_i^2}$; (4) $\frac{\rho_i}{1+\rho_i^2}$; (5) $|\frac{d\rho_i}{dz}|$; (6) $2\rho_i|\frac{d\rho_i}{dz}|/(1+\rho_i^2)^2$; (7) $(1-\rho_i^2)|\frac{d\rho_i}{dz}|/(1+\rho_i^2)^2$ [MacLeod 1966].

for the ion drift velocity expressed in equation (22), the divergence contains a contribution proportional to wind shear and a contribution proportional to the gradient of $\rho_i$

$$\nabla.\mathbf{v}_i = \frac{1}{1+\rho_i^2}\{\rho_i^2\nabla.\mathbf{u}+\rho_i\hat{\Gamma}.\nabla\times\mathbf{u}+\hat{\Gamma}.[(\hat{\Gamma}.\nabla)\mathbf{u}]\}+\frac{1}{(1+\rho_i^2)^2}\{2\rho_i[\mathbf{u}-(\mathbf{u}.\hat{\Gamma})\hat{\Gamma}]+(1-\rho_i^2)\mathbf{u}\times\hat{\Gamma}.\nabla\rho_i. \tag{32}$$

In order for a net enhancement of ionization to occur the divergence must be negative. Equation (32) states that such a convergence will exist if one or more of the following conditions occur in the transport process; 1) the neutral wind convergence is positive; 2) the neutral wind vorticity has a substantial component antiparallel to the geomagnetic field; 3) the projection on the geomagnetic field of the directional derivative of the neutral wind vector along the geomagnetic filed is negative; 4) the projection of the neutral wind component parallel to the geomagnetic field on the gradient of $\rho_i$ is negative; 5) The projection of $\mathbf{v}_{im}$ on the gradient of $\rho_i$ is positive (negative) when $\rho_i > 1$ ($\rho_i < 1$); 6) projection of neutral wind on the gradient of $\rho_i$ is negative.

The quantities occurring in the expression for ion drift velocity equation (22) and its divergence equation (32)do not all appear to be of equal importance which allows the expression to be simplified. Introducing a geomagnetically oriented frame with the $y$ directed along geomagnetic north, and $x$ axis along geomagnetic east and $z$ axis directed upward along the local vertical. The horizontal neutral wind components are so greater than the vertical component that is

$$u_z \ll u_x \text{ and } u_z \ll u_y,$$
$$\tfrac{\partial u_z}{\partial z} \ll \tfrac{\partial u_x}{\partial z} \text{ and } \tfrac{\partial u_z}{\partial z} \ll \tfrac{\partial u_y}{\partial z},$$

and the vertical component and its vertical shear may be neglected in comparison with the horizontal components and their vertical shears. The wind components with horizontal distances appears to be of order of magnitude less than the variation of these components with altitude, and the gradient operator may be written as

$$\nabla = \mathbf{k}\tfrac{\partial}{\partial z}.$$

Upon introducing these approximations and assumptions into the divergence of the ion drift velocity it takes the final form as

$$\frac{\partial v_{iz}}{\partial z} = \frac{\Gamma_y}{(1+\rho_i^2)}\{\rho_i\frac{\partial u_x}{\partial z}+\Gamma_z\frac{\partial u_y}{\partial z}+\frac{1}{(1+\rho_i^2)}\frac{d\rho_i}{dz}[-2\rho_i u_y\Gamma_z+(1-\rho_i^2)u_x]\}. \tag{33}$$

The divergence is thus proportional to the horizontal component of the geomagnetic field and decreases in magnitude at least as rapidly as $\rho_i^{-1}$ in the lower E-region. Positive convergence is obtained when $\frac{\partial v_{iz}}{\partial z}$ is negative. In other words, if $v_{iz}$ goes to zero at some altitude then convergence is obtained when the ions above this level are moving down ward while the ions below are moving upwards. Positive convergence may be obtained in four ways: 1) if the first term in equation (33) dominates and geomagnetic west-east shear is negative (the east-ward wind decreases with altitude); 2) if the second term dominates and the geomagnetic south-north shear is positive (negative) [the northward wind increases (decreases) with altitude] in the northern (southern) hemisphere; 3) if the third term dominates a northward (southward) wind is found in the northern (southern) geomagnetic hemisphere; or 4) if the fourth term dominates and a westward (eastward) wind is found for $\rho_i > 1$ ($\rho_i < 1$).

Theoretical establishment of the wind shear theory is well developed and its consistency with observation will be reviewed later and also it will be investigated numerically. Before coming to the numerical investigation a through study of recent rocket observation is to be reviewed in the next chapter.

# CHAPTER 3

# RECENT ROCKET OBSERVATION OF SPORADIC-E LAYERS

## 3.1 Introduction

A series of rocket flights launched from the NASA Wallops Island Flight Facility, VA (37.84 N, 75.48 W) on 30 July 2003, were carried out to investigate E-region enhanced layers between 100 and 150 km. The experiment had three primary objectives. The first two were to measure the long period time variation of the plasma density and horizontal neutral winds associated with the enhanced layers. The third objective was to measure the relative ion composition of secondary peaks and sporadic-E layers.

Over the past 50 years approximately 50 rocket-borne ion mass spectrometry have sampled the metal ion population between 80 and 130 km [Grebowsky and Aikin, 2002] cited with in [Roddy 2005]. The data set presented here represents the only documented rocket flight of an ion mass spectrometer through a nighttime E-region.

Although the rockets launched from Wallops island were to investigate E-region layers other than sporadic-E layers. Since the trajectories of the rockets traverses through sporadic-E layers it was possible to study them. The observations obtained simultaneous measurements of electron density, neutral wind profile, relative composition of molecular and metallic ions, and electric field profile.

Four rockets were launched at intervals of up to two hours over the course of one night. The four payloads were launched into significant Sporadic-E conditions as monitored by the Wallops digital ionosonde. Geomagnetically moderate conditions existed with $F_{10.7} = 118.4 \times 10^{22} W m^{-2} H z^{-1}$, sunspot number of 94, and Kp 3hr average of 4.

Three of the four payloads carried neutral wind and electron density measuring instruments. Each payload were launched at times 23:19, 01:41, and 03:07 LT. The fourth payload launched at 02:50 LT, carried measurements of electric field and relative composition of molecular and metallic ions.

## 3.2 Observation and Discussion

Figure 7 shows the sequential electron density profiles measured by the four rockets. Both a sporadic-E layer centered at 103 km and a secondary peak centered at 120 persist throughout the night.

The measurement of relative concentration of metallic and molecular ions for sporadic-E layers and secondary peaks are shown in Figure 8. The sporadic-E layer is composed primarily of metallic species while secondary peaks comprises a thin layer of metals superimposed on a broader layer of $NO^+$. On the upleg (downleg), $NO^+$ accounts for 55%(35%) for the secondary peak column density between 114 and 118 km (116 and 120 km) while $Fe^+$ and $Mg^+$ account for 33% (30%) and 10% (35%) respectively. In contrast, the relative composition of the sporadic-E layer between 101 and 107 km (100 and 106 km) is 2.3%(2.5%) $NO^+$, 84%(77%) $Fe^+$, and 13%(21%) $Mg^+$. The $O_2^+$ concentration is on the order of $10cm^{-3}$ below 140 km and changes in its density are not well correlated to the layering events.

Three of the rockets were instrumented with horizontal wind measuring devices. The instruments provided horizontal wind profile. Figure 9 shows the upleg wind profile. The electric field measuring instrument was aboard on the fourth rocket. The data set obtained is displayed in Figure 10. The relevant parameters of wind shear theory were measured by the rocket campaign, which would help alot in investigating the theory to cheek validity of the wind shear theory.

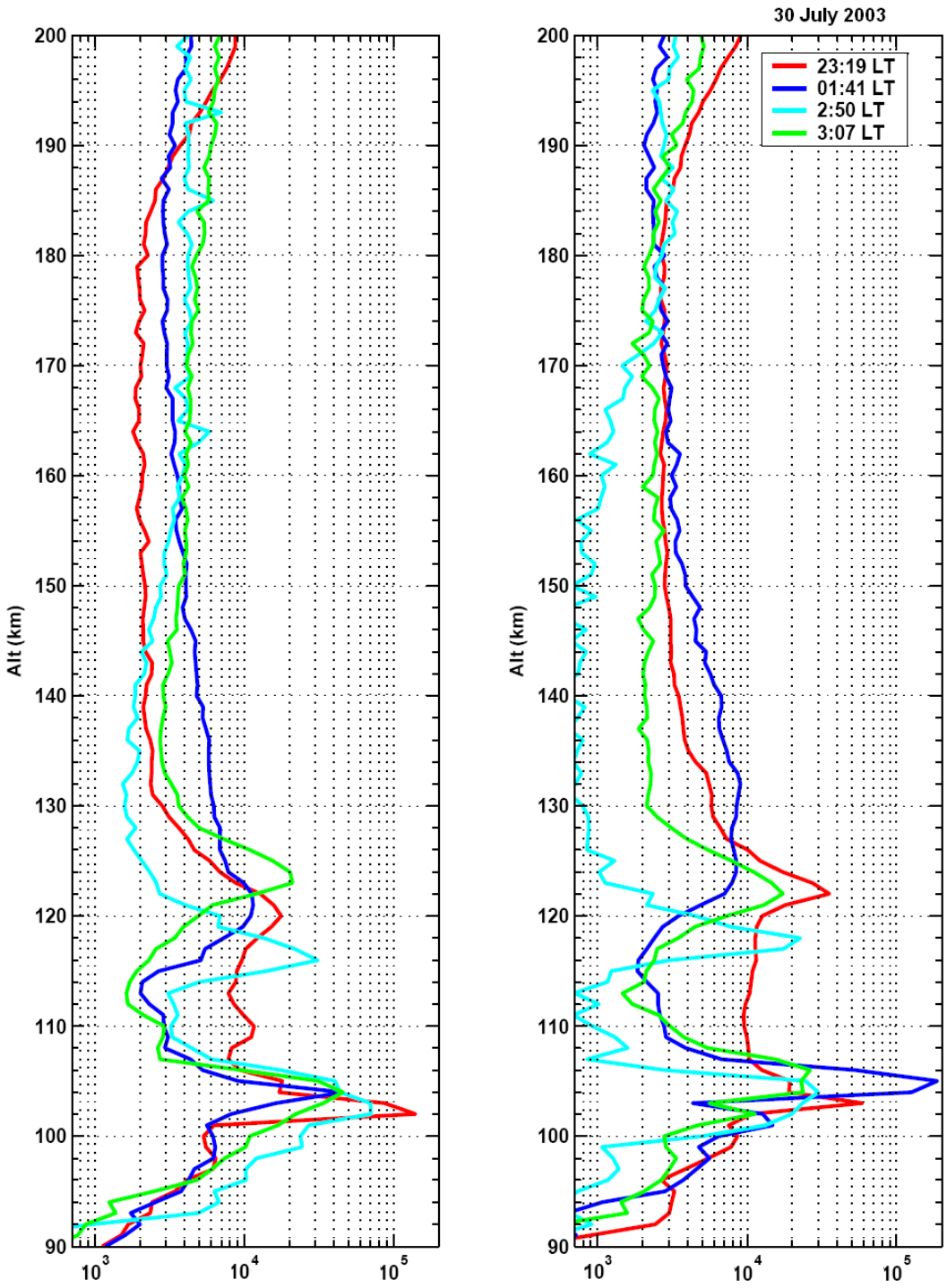


Figure 7: Electron density profile for both up (left) and down (right) legs [Roddy 2005].

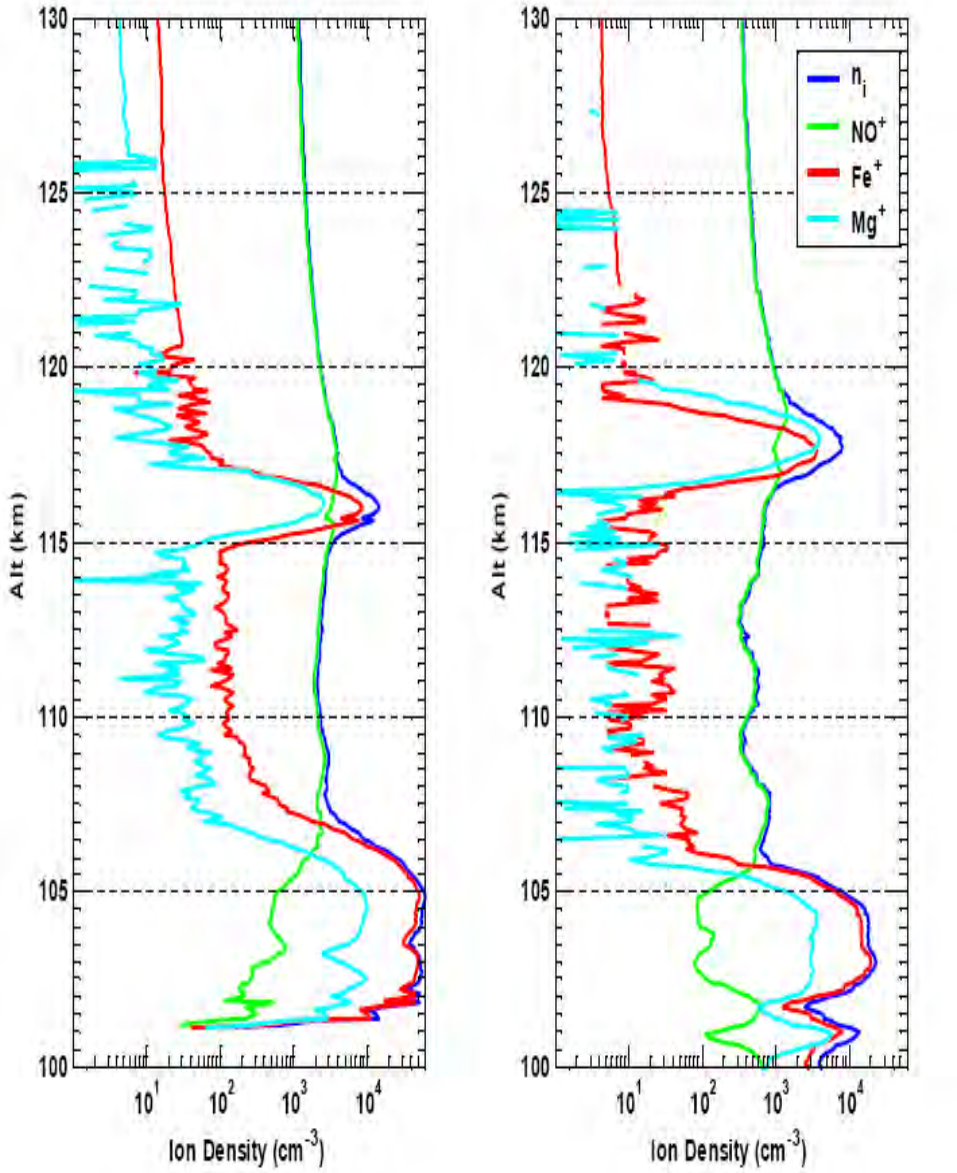


Figure 8: Relative composition of metallic and molecular ions showing sporadic-E layers and secondary peaks for both up(right) and down(left)legs. $n_i$ is the total ion density [Roddy 2005].

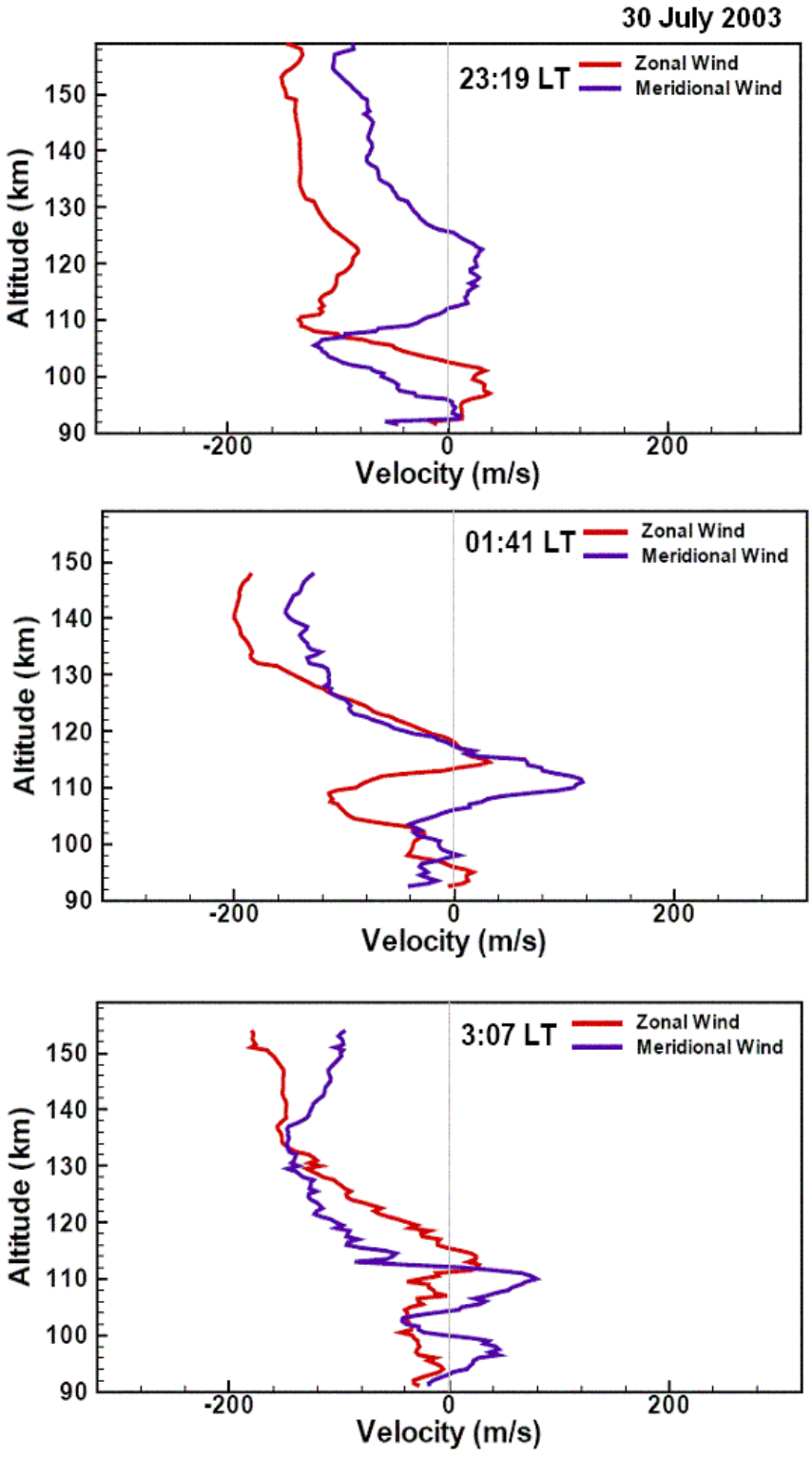


Figure 9: Wind Profile from upleg [Bishop 2005].

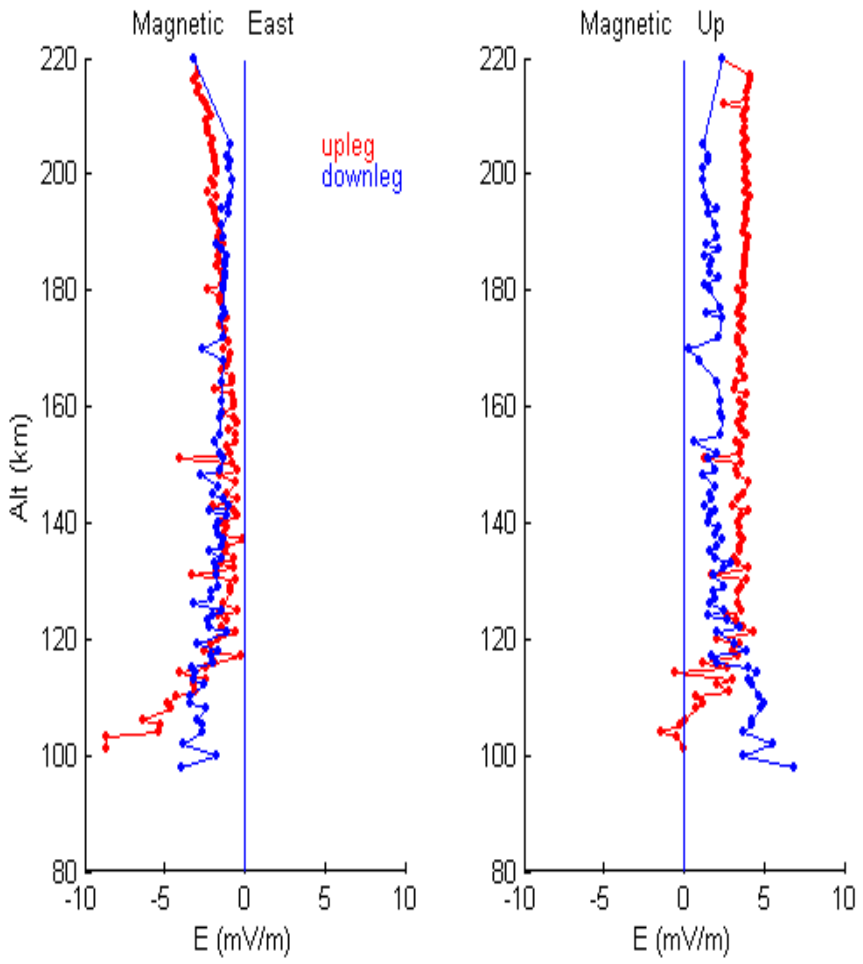


Figure 10: Electric field profile from both up (left) and down (right) legs [Roddy 2005].

# CHAPTER 4

# NUMERICAL INVESTIGATION OF WIND SHEAR THEORY

Numerical investigations of sporadic E-layer may be traced back to [Chimonas and Axford 1968] as cited within [Carter and Forbes, 1997], and [MacLeod 1975]. Their numerical results validated the hypothesis that Sporadic-E layers are caused by the accumulation of metallic ions in convergent nulls in the vertical ion drift coupled with neutral wind profile. These studies did not consider the effects of gravity, electric fields, metallic and ambient ion chemistry, or any serious consideration of the metallic ion source. With the inclusion of all of these parameters [Carter and Forbes 1997] carried out numerical study and concluded that the effects of gravity and ion chemistry have minimal impact on the layer formation. They also found out that electric field effects could offset or enhance layer formation. In this thesis we present results of numerical calculations using wind shear theory. We have also incorporated effects of electric fields.

## 4.1 Numerical Investigations of Wind Shear Theory

The temporal and spatial evolution of electron density (denoted here by $n(\mathbf{r},t)$) in the ionosphere may be expressed by

$$\frac{\partial n(\mathbf{r},t)}{\partial t} = -\nabla.(n(\mathbf{r},t)\mathbf{v(r,t)}) + q(\mathbf{r},t) - l(\mathbf{r},t) + \nabla.(D\nabla n(\mathbf{r},t)), \tag{34}$$

where $\mathbf{v(r,t)}$ is the drift velocity of the plasma, $q(\mathbf{r},t)$ and $l(\mathbf{r},t)$ is the production and loss rates, respectively, D is the coefficient of diffusion (assumed constant), and $\mathbf{r}$ is the three dimensional position vector. The quantity $n(\mathbf{r},t)\mathbf{v(r,t)}$) is referred to as the advective flux and $D\nabla n(\mathbf{r},t)$ represents the diffusive flux. Equation (34) tells us that the rate of change of the electron density is diminished by the net outward flux due to drift and diffusion, increased by the local rate of electron production, and decreased by the local rate of electron loss.

For middle latitude ionosphere, one may use the following assumptions to simplify the model. Since the horizontal extent of sporadic-E layer is of the order of hundreds

of kilometers, the horizontal variation of all quantities can be neglected. The number density of electrons is equal to the total sum of number densities of positive ions. From rocket observation metallic ions have been seen to be the dominate species of all other constituent ions in sporadic-E layers. This means that the production and loss terms in equation (34) can be neglected. This is because of the longer life times for the metallic ions under consideration. Lastly, the diffusion term is unimportant except for very narrow layers.

Making use of all these assumptions and denoting the vertical direction by z-axis equation (34) reduces to

$$\frac{\partial n(z,t)}{\partial t} + \frac{\partial (n(z,t)v_i(z,t))}{\partial z} = 0. \tag{35}$$

Here we have replaced plasma velocity by the ion drift velocity. We have found an explicit expression for the vertical component of the ion drift velocity (along z-axis) in section 2.5.1, which can be used in equation 35.

### 4.1.1 Numerical Scheme

Equation 35 can be solved numerically by employing the finite difference (Lax-Friedrichs Scheme). Let us introduce a function $f(z,t)$ such that

$$f(z,t) = n(z,t)v_i(z,t)). \tag{36}$$

This means that we can re-write equation 35 as

$$\frac{\partial n(z,t)}{\partial t} + \frac{\partial f(z,t)}{\partial z} = 0. \tag{37}$$

When we employ forward in time and centered in space (FTSC) partition scheme, we can obtain

$$n(z,t+\Delta t) = n(z,t) + \frac{\Delta t}{2\Delta z}[f(z+\Delta z,t) - f(z-\Delta z,t)], \tag{38}$$

where $\Delta t$ is the temporal resolution $\Delta z$ is the spatial resolution. One can obtain the spatial and temporal evolution of electron density from the difference equation 38. However, the numerical estimate may be improved by using average of the neighboring spatial grid points. This means that (38) by

$$n(z,t+\Delta t) = \frac{1}{2}[n(z+\Delta z,t) + n(z-\Delta z,t)] + \frac{\Delta t}{2\Delta z}[f(z+\Delta z,t) - f(z-\Delta z,t)]. \tag{39}$$

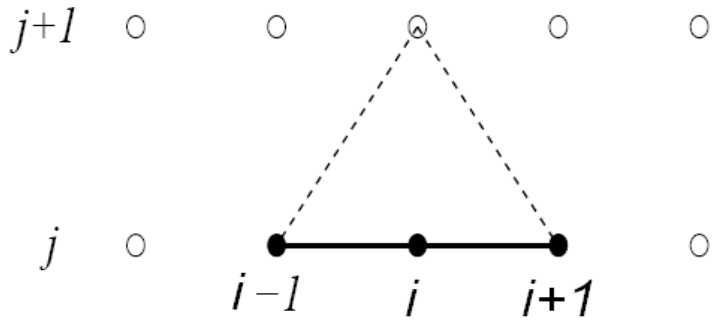


Figure 11: Schematic diagram of Lax-Friedrichs evolution scheme.

Let us introduce $i$ and $j$ to denote spatial and temporal variables as subscript in such a way that $t = j$, $z = i$ and each step in temporal and spatial is considered as one. This means that we can re-write equation (39) by

$$n_{i,j+1} = \frac{1}{2}(n_{i+1,j} + n_{i-1,j}) + \frac{1}{2}c(f_{i+1,j} - f_{i-1,j}), \tag{40}$$

where $c = \frac{\Delta t}{2\Delta z}$ (the stability (Courant condition) can be checked if $c \leq 1$ and the value of c in this study is $5 \times 10^{-5}$ ). The numerical scheme in equation 40 may be understood better by using a schematic diagram. Figure 11 shows that three grid points having the same temporal grid value but different spatial grid values are used to calculate the value of one grid point which is one step ahead in time.

### 4.1.2 Initial Conditions and Assimilated Data

In order to solve equation (40) numerically, we have used an initial plasma density profile and also measured wind profile. Figure 12 shows the initial profile used in our calculation (note that the dominant metallic ion which is $Fe^+$ is nearly equal to the electron density profile).

In sporadic E layer region the neutral gas and ions are coupled via collision, the wind velocity is incorporated in the equation of evolution of electron density profile. We have used the wind velocity measured by rocket [Roddy 2004]. The measured horizontal wind profile has a grid spacing of $1km$. However, some data points are missing and we have used polynomial interpolation to estimates for these values.

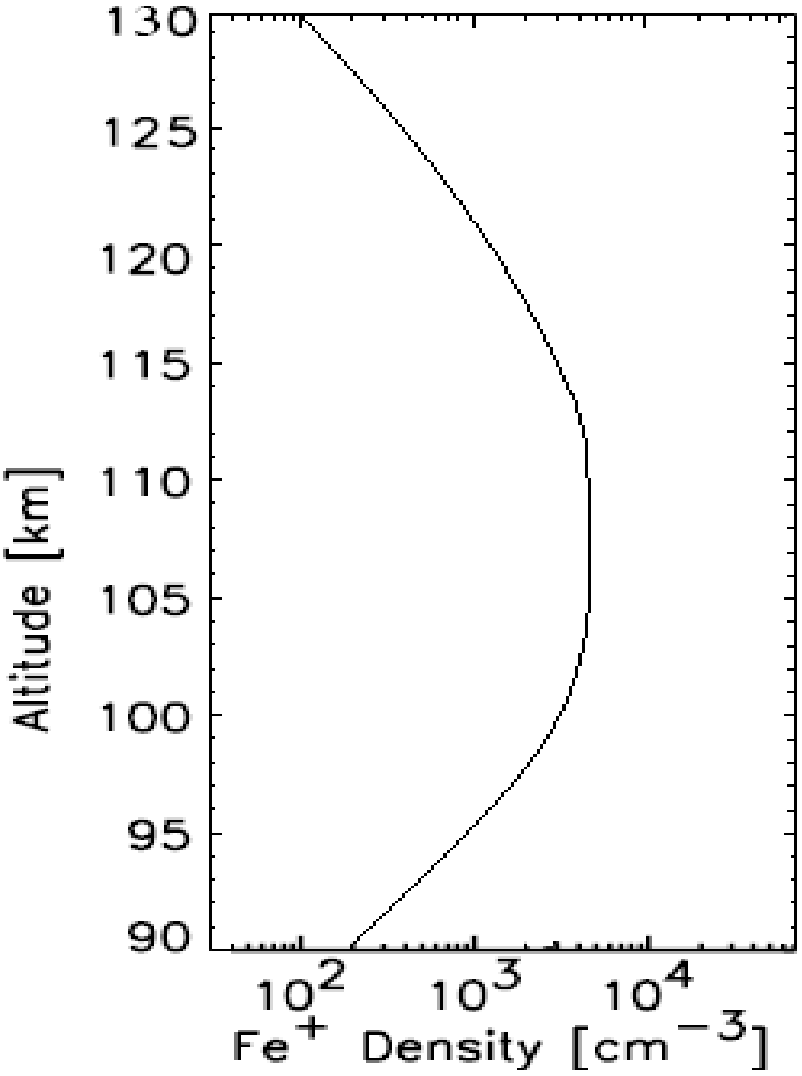


Figure 12: Initial distribution of metallic ion density.

### 4.1.3 Numerical Solution

Using the above initial condition and data assimilated, we have been able to obtain numerical solutions. First we present a simulation of the formation of sporadic-E layers by considering the neutral wind effects only. A coordinate axis is fixed with east defined as positive $x$, north as positive $y$, and up as a positive $z$.

According to the wind shear theory, mid-latitude sporadic-E layers form through a combination of horizontal neutral winds and the underlying magnetic field geometry. Ions experience motion through collisions via meridional neutral wind field, they are also constrained to move along the inclined geomagnetic field. This produces ion motion containing a vertical component. In order to produce a region of convergent drift, a shear in the meridional wind, defined as a poleward directed wind above and an equator-ward wind directed below the region of interest, must exist. A similar scenario for producing ion layers can be developed for zonal neutral winds with the principal force provided by $\mathbf{v} \times \mathbf{B}$, where $\mathbf{v}$ is the ion velocity. In this case, the zonal wind shear must be directed westward above the layer and eastward below. When viewing neutral wind profiles as a function of height, the direction of any gradient with respect to altitude indicates the presence of a convergent or divergent shear in the resulting vertical ion motion. The condition for the formation of a plasma layer is a positive or negative sloped gradient (shear) with respect to altitude in the meridional or zonal neutral wind fields, respectively. Other combinations of wind shears, such as a northward meridional wind and an underlying eastward zonal wind, can also produce a region of plasma buildup. Thus both horizontal wind components must be considered at all altitudes to calculate the net vertical plasma drift and consequently to determine regions of plasma convergence.

Figures 13 and 14 display the data obtained from measurement. Figure 13 shows the zonal and meridional neutral wind profiles as a function of altitude. The gray boxes indicate regions of convergent shears within the individual neutral wind component. For example, a zonal neutral wind containing a shear with a negative slope results in ion motion that causes the ions to be compressed into a layer near the center of the shear region. Figure 13 shows at least two convergent regions within each zonal neutral wind profile. The meridional neutral wind profiles contain fewer convergent shear regions within the observed altitude range. The derived vertical ion velocity profiles are shown in Figure 14. The vertical ion velocity profiles are calculated following the procedure outlined in section 2.5.1 Chapter two. The calculated ion drift profiles in Figure 14 results when the

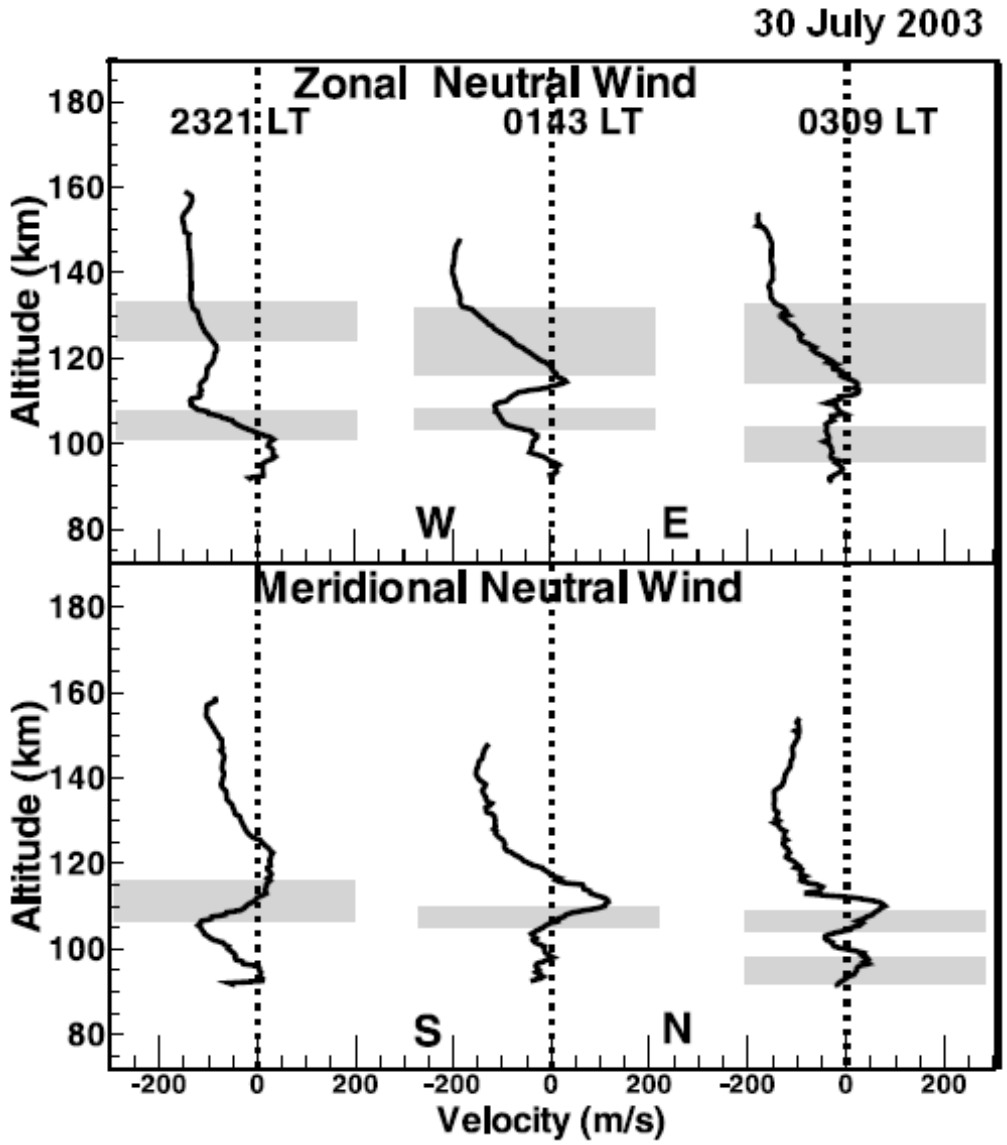


Figure 13: The top and bottom show the upleg zonal and meridional neutral wind profiles observed from three separate chemical release experiments, respectively. The shaded boxes indicate the convergent shear region.[Bishop 2005]

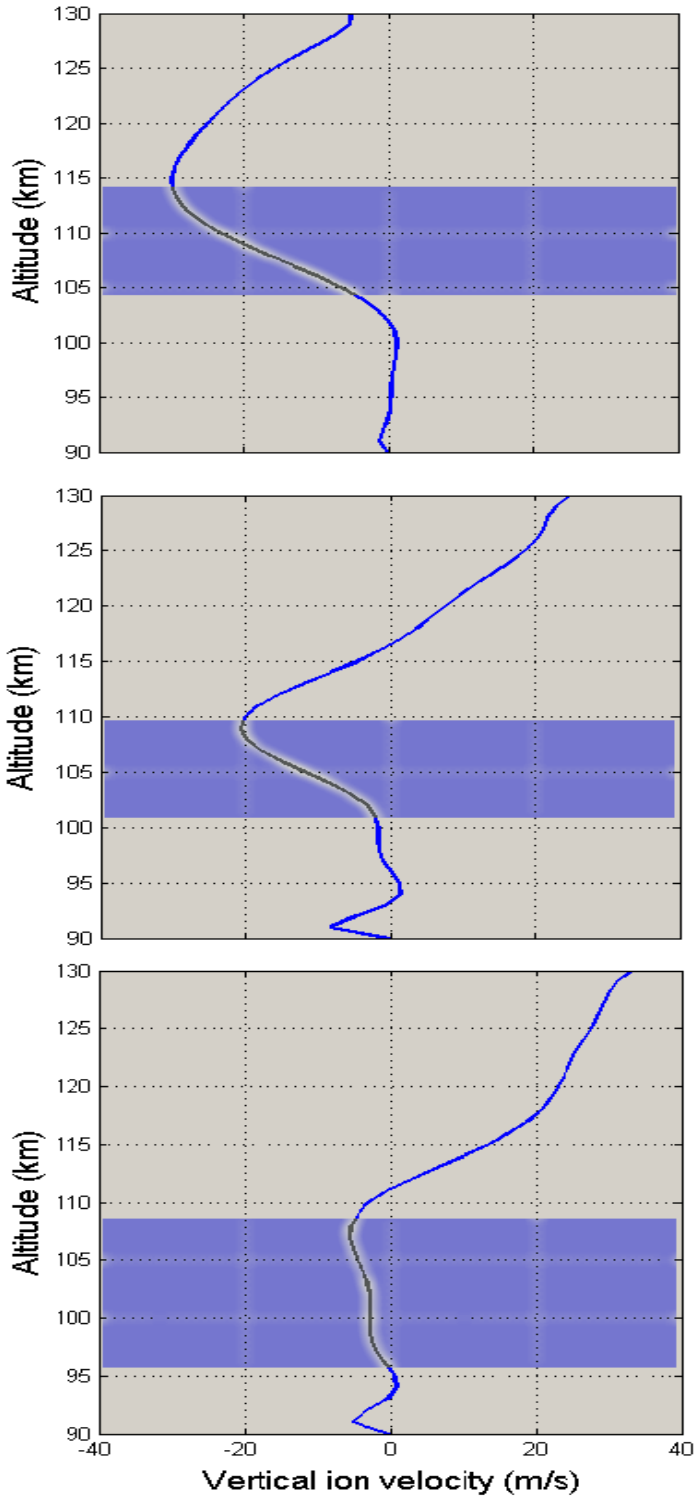


Figure 14: Vertical ion velocity profule calculated form neutral wind effect.

neutral winds shown in Figure 13 are used as input. The corresponding calculated density of metallic ions profiles are shown in Figure 15. The gray boxes in Figure 14 indicate regions of convergent ion motion. The simulation results are displayed in 3D plots, as a function of time and altitude.

In the relevant shear convergent regions shown in Figure 14 sporadic-E layers are formed with a very short simulation times $200 - 300sec$. The density data measured by rocket is shown in Figure 16. In each density profile, two significant layers are observed between 90 and 130 km. Over the span of several hours, the two layers remain nearly stationary but become more clearly defined and isolated. Sporadic-E layers are situated at an altitude $103km$, and secondary peaks are situated in a range of $120 - 130km$ for all times. The simulation results obtained by incorporating the vertical drift in Figure 14 show sporadic-E layers situated in range of $106 - 112km$. Two major discrepancies are observed when comparing simulation results in Figure 15 and observation in Figure 16. The first one is that the layers are observed at a little higher altitude in the simulation results. The second one is that there is no convergent shear region in Figure 14 for the observed secondary peak, and obviously no secondary peaks exist in the corresponding simulation result shown in Figure 15.

In general, the sporadic-E layers and the regions of convergent shears due only to the horizontal wind are in agreement. The secondary peaks are much more complicated. The neutral wind fields alone are not capable of producing the observed secondary peaks. The following discussion explores other factors that may further improve the agreement between the secondary peaks and convergent shear regions in the vertical drift profiles. The wind shear formation theory for plasma layers predicts that a meridional neutral wind is more efficient at producing ion motion above 130 km and a zonal neutral wind is more efficient below 120 km. This is due to the altitude dependence of the ion gyrofrequency and collision frequency and their coupling to the neutral wind components in the vertical ion velocity calculation. The altitude range from 120 to 130 km is a transition (mixed) region where the zonal and meridional wind components are equally efficient at producing ion motion. The secondary peaks observed in this experiment was contained in the transition region over the entire observation period. The location of the secondary peaks in the transition region complicates the explanation of the significant differences observed between the location of the secondary peaks and convergent drift regions. There are three possible geophysical reasons for the large observed discrepancies. They are (1) electric field induced vertical

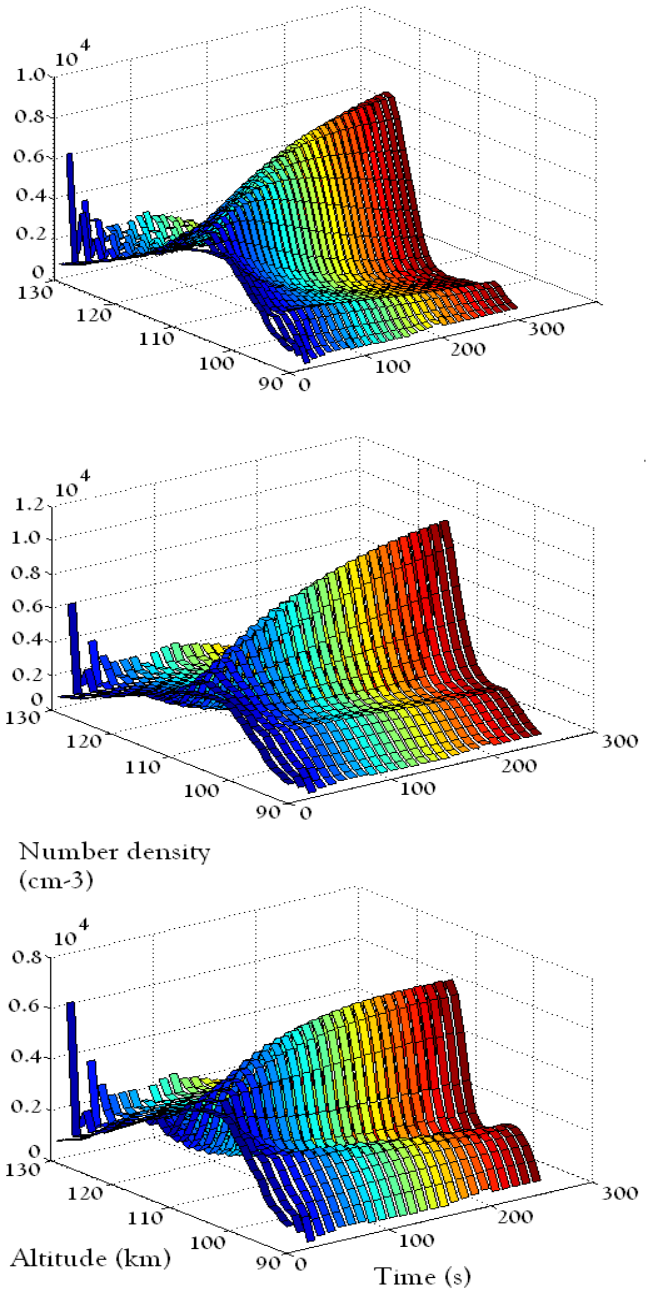


Figure 15: Simulation results upon application of the observed wind for all times.

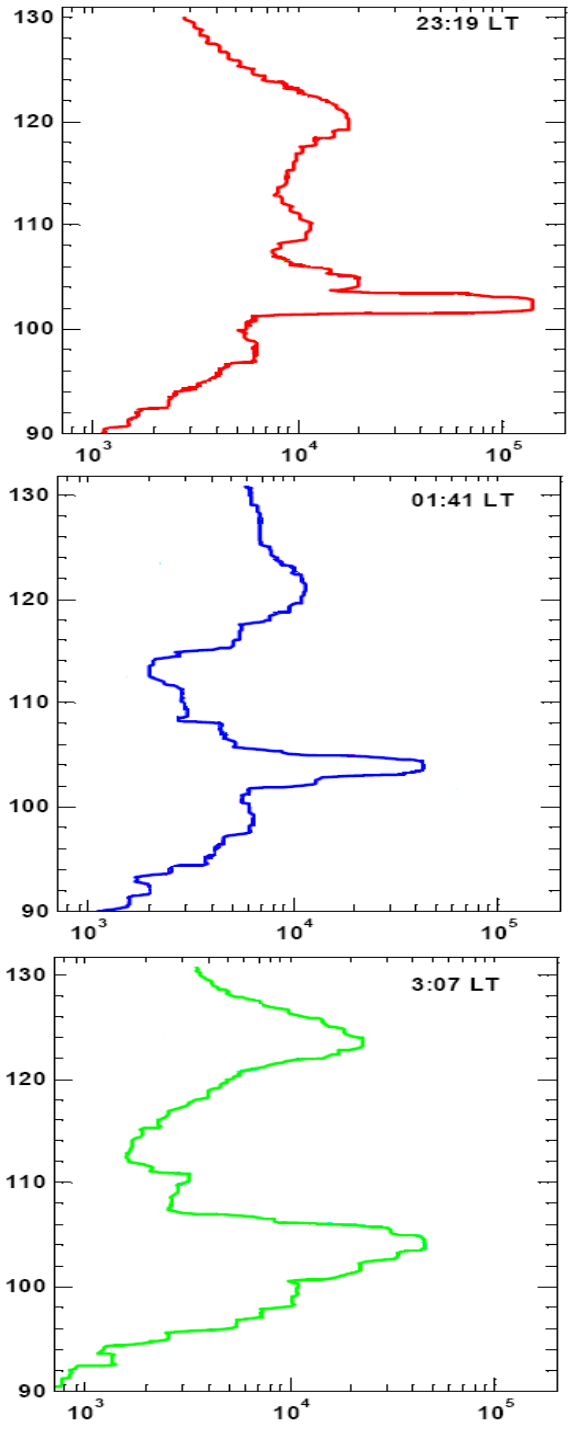


Figure 16: Observed electron density profile.

transport, (2) variations in the mean collision frequency,(3) contributions to the vertical ion motion by a vertical neutral wind.

In most calculations and modelling efforts, the contribution of the vertical neutral wind to ion motion is neglected. Vertical neutral winds are very efficient at producing vertical ion motion, but are inherently difficult to determine, and were not measured in this rocket experiment and may partially explain the large offsets in discrepancies of convergent drift regions in comparison with observation.

Upon addition of altitudinal variation of the ratio of ion collision frequency to gyrofrequency in the calculation of vertical drift velocity the altitudinal variation of the ratio is small to account for the discrepancies of convergent drift region. The variation of mean collision frequencies is mainly dominated by the variation of horizontal neutral wind. We can conclude that this geophysical reason is not responsible to explain the large discrepancies.

Electric field effects are often used to explain unusual changes. Upon addition of electric field on equation (22) the ion drift velocity is written as

$$\mathbf{v}_i = \frac{1}{1+\rho_i^2}[\rho_i^2\mathbf{u} + \rho_i\mathbf{u}\times\hat{\Gamma} + (\mathbf{u}.\hat{\Gamma})\hat{\Gamma}] + \frac{1}{1+\rho_i^2}[\rho_i\mathbf{E} + \mathbf{E}\times\hat{\Gamma} + (1/\rho_i)(\mathbf{E}.\hat{\Gamma})\hat{\Gamma}]. \qquad (41)$$

Where $\mathbf{E} = \mathbf{E}/B_0$.

Figure 17 shows vertical drift velocity calculated by incorporating a steady electric field and neutral wind fields. With the addition of the electric field term, a convergent drift region in the range of $120 - 125km$ for all calculations of vertical drift is observed, corresponding to the location of the observed second peak. The simulation results obtained by incorporating these vertical drift velocity is shown in Figure 18. The results show that sporadic-E layers are unaffected by the inclusion of electric field. Sporadic E layers maintained their pervious locations, this may further investigated by comparing shear regions obtained from the neutral wind fields and added electric field. Though a convergent shear regions were obtained for the secondary peaks by the effect of electric fields, the discrepancies seen in the location of sporadic-E layers still remains unanswered. Simulation results obtained by including electric field effect shows that secondary peaks lie in a range of $120 - 125km$ which is consistency with observation shown in Figure 16.

None of the three explanations presented can completely account for the offsets between the observed the centers of the sporadic-E layers and vertical ion motion of the shears. However, a vertical neutral wind, an appropriately directed electric field, could

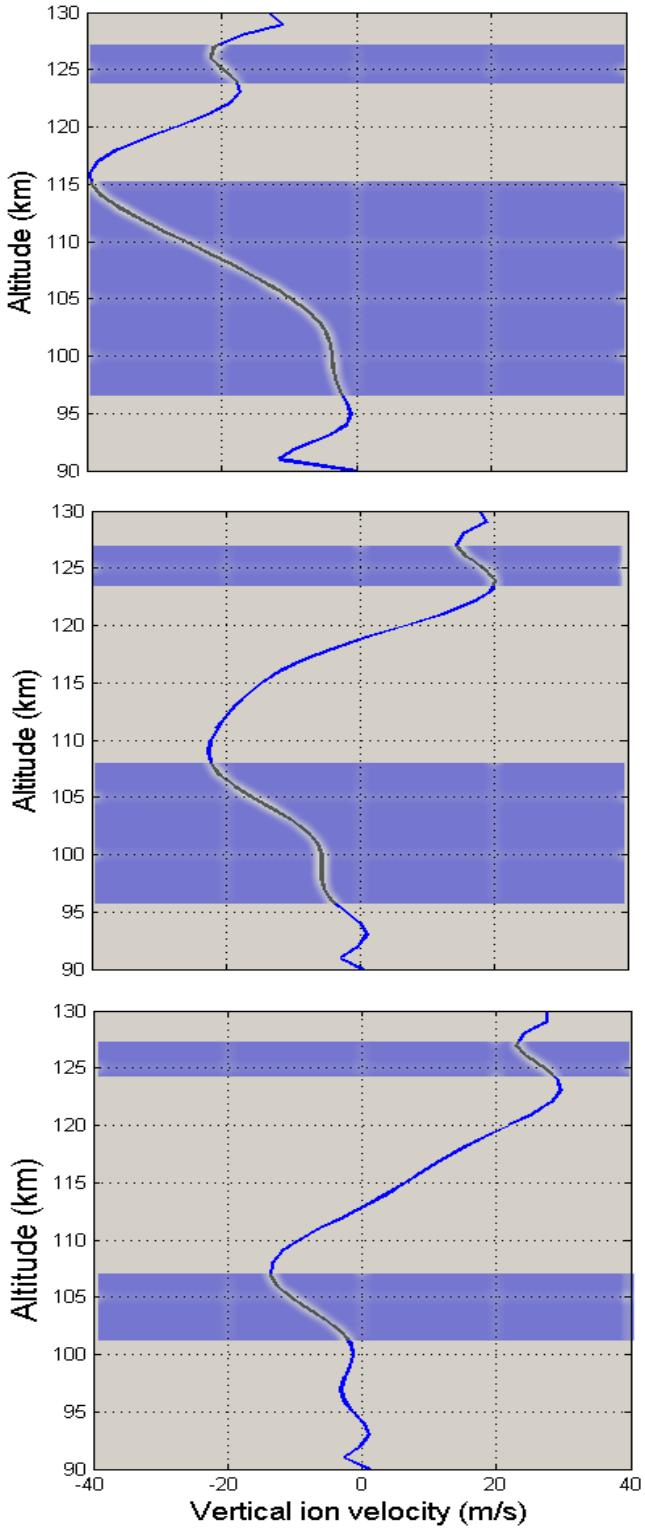


Figure 17: Vertical wind velocity profile obtained from both electric and wind fields.

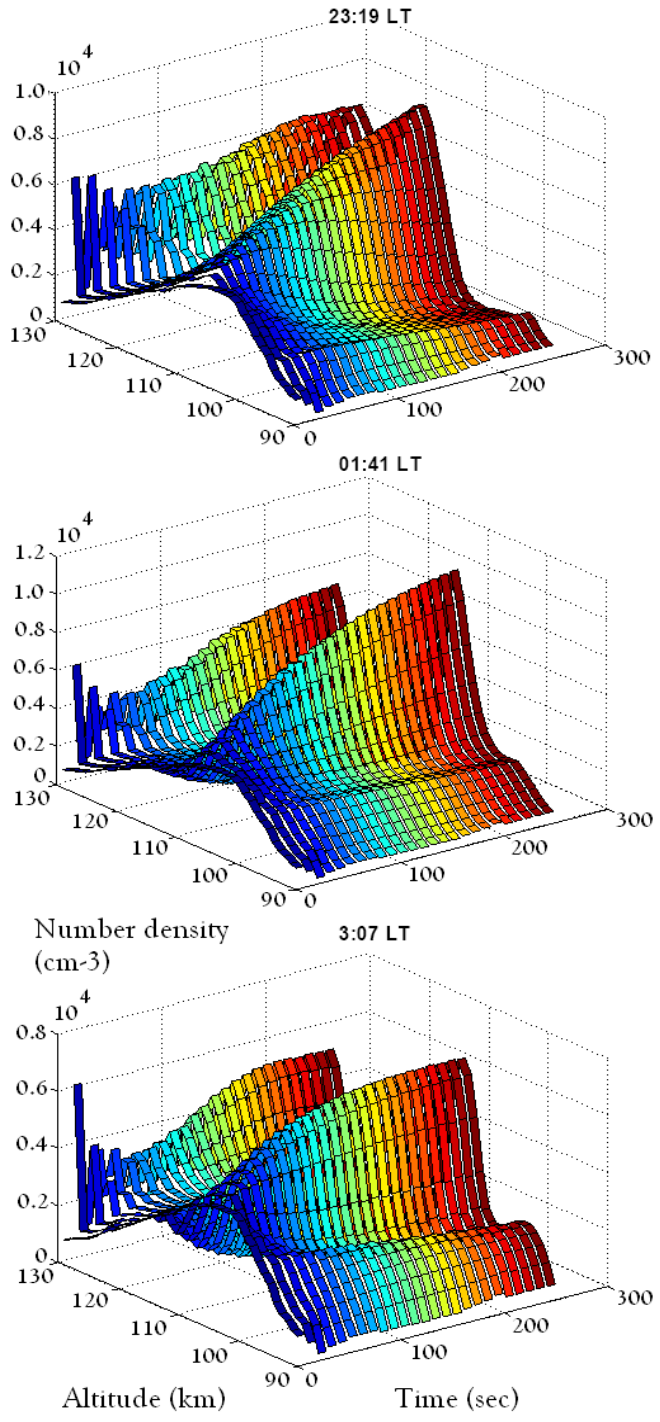


Figure 18: Simulation results upon the application of constant electric field and wind fields for all times.

produce any individual offset observed. It may be a combination of the two effects which is responsible for the offsets observed between the drift nulls and the altitude of the sporadic-E layers. Although we were able to attain the second peak upon addition of electric field effect on the first simulation result from neutral wind effect, there exist other inconsistency with the observation. From the observation we can clearly see that peak number density keeps decreasing with time unlike the simulation results. No geophysical reason under consideration can explain this inconsistency and it is attributed to numerical limitation.

## 4.2 Summary and Conclusion

Three rockets containing chemical tracer experiments and plasma impedance probes were launched from Wallops Island. The instruments provided electron density and horizontal neutral wind profiles. A forth rocket was also launched to investigate the electric field profile and relative concentration of ions in addition to electron density and neutral wind. Two plasma layers, a sporadic E layer and a secondary peak, were observed on both the up-going and down-going portions of all three flights. From the neutral wind profile we were able to see convergent regions or possible layer regions in the vicinity of the layers observed. However, inconsistency between the center of the layer and the convergent shear regions resulting from the horizontal neutral winds exist with no second peaks in simulation results.These discrepancies are significantly reduced when a measured electric field is included in the calculations with a clear secondary peak in simulation results.

The wind shear theory was originally created to explain sporadic-E layers, but it has also been applied to secondary peaks at higher altitudes with some success. It is now generally accepted that shears in the horizontal neutral wind produce secondary peaks and that their regular nightly occurrence is due to tidal winds. However, the large variations observed in secondary peaks imply that other factors besides tidal winds may exert considerable influence on their formation and evolution. These factors include composition, gravity waves, and local electric fields.

## 4.3 Future Directions

Having made these initial advances in building on the theoretical foundation, a high potential exists for future contributions. The inclusion of gravity wave field superimposed on the current tidal wind field may allow to fulfill the discrepancies of convergent shear

region of simulation results with observation.
The second peak displayed the most significant variation in bulk composition between up and downlegs. Over a horizontal distance of 130 km and an elapsed time of 5 minutes, the relative column density of the second peak transitioned from being composed of a majority of molecular ions to one that was a majority of metallic ions see Figure 8. At the same time, $Mg^+$ transitioned from the minority metallic species to the dominant ion within the layer column.

Metal ion concentrations have long been known to be patchy within sporadic-E layers, but this observation is the first evidence that secondary peaks may exhibit the same patchy distribution. The increase in relative concentration and column density of $Mg^+$ within the second peak between up and downlegs can either be explained by an initially non-uniform distribution of metal species, a horizontal redistribution of ions due to horizontal gradients in the neutral wind, or a combination of both factors. Are these composition variations acceptable given the wind shear theory of layer formation or do they indicate shortcomings in the theory? this must be further investigated.

# APPENDIX A

# SOURCE CODES

## A.1 Source code used to attain number density profile by the effect of wind at 23:19,01:41,03:07

```
      REAL N(60,60),UX(60),UY(60),VIZC(60,60)
      REAL Z(50)
      OPEN(4,FILE='AT1v.DAT',STATUS='UNKNOWN')
      DATA(UX(I),I=1,41)/  !Put zonal wind data here.

      DATA(UY(I),I=1,41)/ !Put meridional wind data here
       !Give the initial and boundary conditions here.

      DO J=1,25
      DO I=2,39
      Z(I+1)=Z(I)+1
      VIZC(I,J)=(GY/(1+RHO(Z(I))**2)*(RHO(Z(I))*100*UX(I)
     $  +GZ*100*UY(I)))
      VIZC(I+1,J)=(GY/(1+RHO(Z(I+1))**2)*(RHO(Z(I+1))*100*UX(I+1)
     $  +GZ*100*UY(I+1)))
      VIZC(I-1,J)=(GY/(1+RHO(Z(I-1))**2)*(RHO(Z(I-1))*100*UX(I-1)
     $  +GZ*100*UY(I-1)))
      N(I,J+1)=0.5*(N(I+1,J)+N(I-1,J))-0.5*C*(N(I,J)*(VIZC(I+1,J)
     $  -VIZC(I-1,J))+VIZC(I,J)*(N(I+1,J)-N(I-1,J)))
      END DO
      END DO
      DO I=1,40
      WRITE(4,*)(0.01*vizc(I,J),J=1,25)
      END DO
```

```
END
FUNCTION RHO(Z)
RHO= EXP(27.2 - 0.32*Z+0.824*10**(-3*Z**2))
RETURN
END
```

## A.2 Source code used to attain number density by the effect of both neutral wind and electric field at alltimes

```
REAL N(60,60),UX(60),UY(60),VIZC(60,60)
REAL Z(50),EX(60),EY(60)
OPEN(4,FILE='AT3fv.DAT',STATUS='UNKNOWN')
DATA(UX(I),I=1,41)/! Put zonal wind data here.
DATA(UY(I),I=1,41)/ ! Put meridional wind data here.

DATA(EX(I),I=1,41)/ !Put the northward electric field
                      !data here.

DATA(EY(I),I=1,41)/ ! Put the northward electric field
                   ! data here.
!Give your initial and boundary conditions here.
DELT=10.00
GZ=SIN(65.00)
GY=COS(65.00)
DELZ=100000.00
C=(DELT)/(DELZ)
Z(1)=90
Z(2)=91
DO J=1,30
DO I=2,39
   Z(I+1)=Z(I)+1
```

```
   VIZC(I,J)=(GY/(1+RHO(Z(I))**2)*(RHO(Z(I))*100*UX(I)
$  +GZ*100*UY(I))+0.0025*EX(I)-(GZ/RHO(Z(I)))*0.0025*EY(I))
   VIZC(I+1,J)=(GY/(1+RHO(Z(I+1))**2)*(RHO(Z(I+1))*100*UX(I+1)
$  +GZ*100*UY(I+1))+0.0025*EX(I+1)-(GZ/RHO(Z(I+1)))*0.0025*EY(I+1))
   VIZC(I-1,J)=(GY/(1+RHO(Z(I-1))**2)*(RHO(Z(I-1))*100*UX(I-1)
$  +GZ*100*UY(I-1))+0.0025*EX(I-1)-(GZ/RHO(Z(I-1)))*0.0025*EY(I-1))
   N(I,J+1)=0.5*(N(I+1,J)+N(I-1,J))-0.5*C*(N(I,J)*(VIZC(I+1,J)
$  -VIZC(I-1,J))+VIZC(I,J)*(N(I+1,J)-N(I-1,J)))
   N(I,J+1)=(N(I,J+1))
   END DO
   END DO
   DO I=1,40
   WRITE(4,*)(N(I,J),J=1,25)
   END DO
   END
   FUNCTION RHO(Z)
   RHO= EXP(27.2 - 0.32*Z+0.824*10**(-3*Z**2))
   RETURN
   END
```

## A.3 Sample source code with data and initial and boundary conditions

```
     REAL N(60,60),UX(60),UY(60),VIZC(60,60),EX(60),EY(60)
  REAL Z(50)
   OPEN(4,FILE='AT1fv.DAT',STATUS='UNKNOWN')
  DATA(UX(I),I=1,41)/
*   -20.00,
*   -10.00,
*     0.00,
*    10.00,
*     9.00,
```

```
*     0.00,
*    25.00,
*    35.00,
*    45.00,
*    35.00,
*    25.00,
*    30.00,
*    10.00,
*   -10.00,
*   -30.00,
*   -52.00,
*   -72.00,
*   -90.00,
*  -110.00,
*  -120.00,
*  -135.00,
*  -120.00,
*  -110.00,
*  -107.00,
*  -105.00,
*  -102.00,
*  -100.00,
*   -98.00,
*   -94.00,
*   -92.00,
*   -90.00,
*   -85.00,
*   -80.00,
*   -90.00,
*  -100.00,
*  -105.00,
*  -115.00,
*  -125.00,
```

```
*  -130.00,
*  -135.00,
*  -140.00/



  DATA(UY(I),I=1,41)/
*  -50.00,
*  -49.00,
*  -48.00,
*  -47.00,
*    0.00,
*    5.00,
*  -20.00,
*  -30.00,
*  -40.00,
*  -45.00,
*  -55.00,
*  -75.00,
*  -95.00,
* -100.00,
* -110.00,
* -115.00,
*  -90.00,
*  -75.00,
*  -55.00,
*  -50.00,
*  -40.00,
*  -25.00,
*  -15.00,
*  -10.00,
*    0.00,
*   15.00,
```

```
*   17.00,
*   19.00,
*   20.00,
*   20.00,
*   20.00,
*   17.00,
*   20.00,
*   10.00,
*    5.00,
*    0.00,
*  -10.00,
*  -20.00,
*  -25.00,
*  -35.00,
*  -40.00/
   DATA(EX(I),I=1,41)/
*    0.00,
*    0.00,
*    0.00,
*    0.00,
*    0.00,
*    0.00,
*    0.00,
*    0.00,
*    0.00,
*    0.00,
*    -7.5,
*   -7.25,
*   -6.75,
*    -6.5,
*   -6.00,
*   -5.75,
*    -5.5,
```

```
*   -5.25,
*   -7.75,
*    -4.5,
*    -2.5,
*   -4.65,
*    -2.5,
*     0.00,
*    -2.6,
*    -2.4,
*    -2.4,
*    -2.5,
*  -2.275,
*   -0.95,
*   -2.25,
*   -1.75,
*   -1.25,
*   -1.75,
*    -1.5,
*    -1.2,
*   -1.00,
*   -1.25,
*    -1.2,
*   -1.00,
*   -0.95/
  DATA(EY(I),I=1,41)/
*   0.00,
* -0.625,
*  -1.35,
*   -0.1,
*   0.00,
*    0.1,
*  0.625,
*   1.25,
```

```
*   1.24,
*  0.625,
*    0.6,
* 0.3125,
*    2.8,
* -0.833,
*   1.25,
*    1.3,
*   3.75,
*   3.75,
*   3.75,
*   3.75,
*   3.75,
*   3.75,
*   3.75,
*   3.79,
*   3.75,
*   3.75,
*   3.76,
*   3.75,
*   3.75,
*   3.75,
*   3.78,
*   3.75,
*   3.75,
*   3.75,
*   3.75,
*   3.75,
*   3.75,
*   3.78,
*   3.75,
*   3.75,
*   3.75/
```

```
N(1,1)=900.00
N(2,1)=1000
N(3,1)=1250
N(4,1)=1395
N(5,1)=1708.7
N(6,1)=2267
N(7,1)=2527
N(8,1)=2851
N(9,1)=3298
N(10,1)=3557
N(11,1)=3985
N(12,1)=4154
N(13,1)=4140
N(14,1)=4145
N(15,1)=4135
N(16,1)=4085
N(17,1)=3963
N(18,1)=3934.00
N(19,1)=3783.00
N(20,1)=3701.00
N(21,1)=3517.00
N(22,1)=3386.00
N(23,1)=3106.00
N(24,1)=3063.00
N(25,1)=2866.00
N(26,1)=2764.00
N(27,1)=2570.00
N(28,1)=2419.00
N(29,1)=2237.00
N(30,1)=2068.00
N(31,1)=1917.00
N(32,1)=1729.00
```

N(33,1)=1732.00
N(34,1)=1457.00
N(35,1)=1300.00
N(36,1)=1100.00
N(37,1)=1000.00
N(38,1)=900.00
N(39,1)=800.00
N(40,1)=700.00
N(1,2)=575.9435
N(1,3)=106.7735
N(1,4)=248.8723
N(1,5)=300.00
N(1,6)=400.00
N(1,7)=400.00
N(1,8)=400.00
N(1,9)=300.00
N(1,9)=300.00
N(1,10)=300.00
N(1,11)=300.00
N(1,12)=280.00
N(1,13)=260.00
N(1,14)=280.00
N(1,15)=270.00
N(1,16)=260.00
N(1,17)=350.00
N(1,18)=400.00
N(1,19)=450.00
N(1,20)=550.00
N(1,21)=400.00
N(1,22)=400.00
N(1,23)=400.00
N(1,24)=400.00
N(1,25)=400.00

```
N(1,26)=400.00
N(1,27)=400.00
N(1,28)=400.00
N(1,29)=400.00
N(1,30)=400.00
N(40,2)=6019.6525
N(40,3)=1022.1929
N(40,4)=3537.2459
N(40,5)=2500.00
N(40,6)=2000.00
N(40,7)=2000.00
N(40,8)=2000.00
N(40,9)=1500.00
N(40,10)=2000.00
N(40,11)=2180.00
N(40,12)=2270.00
N(40,13)=2000.00
N(40,14)=1950.00
N(40,15)=1800.00
N(40,16)=1650.00
N(40,17)=1400.00
N(40,18)=1200.00
N(40,19)=1000.00
N(40,20)=800.00
N(40,21)=1000.00
N(40,22)=1000.00
N(40,23)=1000.00
N(40,24)=1000.00
N(40,25)=1000.00
N(40,26)=1000.00
N(40,27)=1000.00
N(40,28)=1000.00
N(40,29)=1000.00
```

```
      N(40,30)=1000.00
      DELT=10.00
      GZ=SIN(65.00)
      GY=COS(65.00)
      DELZ=100000.00
      C=(DELT)/(DELZ)
      Z(1)=90
      Z(2)=91
      DO J=1,25
      DO I=2,39
      Z(I+1)=Z(I)+1
      VIZC(I,J)=(GY/(1+RHO(Z(I))**2)*(RHO(Z(I))*100*UX(I)
     $  +GZ*100*UY(I))+0.0035*EX(I)-(GZ/RHO(Z(I)))*0.0035*EY(I))
      VIZC(I+1,J)=(GY/(1+RHO(Z(I+1))**2)*(RHO(Z(I+1))*100*UX(I+1)
     $  +GZ*100*UY(I+1))+0.0035*EX(I+1)-(GZ/RHO(Z(I+1)))*0.0035*EY(I+1))
      VIZC(I-1,J)=(GY/(1+RHO(Z(I-1))**2)*(RHO(Z(I-1))*100*UX(I-1)
     $  +GZ*100*UY(I-1))+0.0035*EX(I-1)-(GZ/RHO(Z(I-1)))*0.0035*EY(I-1))
      N(I,J+1)=0.5*(N(I+1,J)+N(I-1,J))-0.5*C*(N(I,J)*(VIZC(I+1,J)
     $  -VIZC(I-1,J))+VIZC(I,J)*(N(I+1,J)-N(I-1,J)))
      N(I,J+1)=(N(I,J+1))
      END DO
      END DO
      DO I=1,40
      WRITE(4,*)(N(I,J),J=1,25)
      END DO
      END
      FUNCTION RHO(Z)
      RHO= EXP(27.2 - 0.32*Z+0.824*10**(-3*Z**2))
      RETURN
      END
```

# Bibliography

[1] Aikin, A. C., J. M. Grebowsky, and J. P. Burrows, Satellite measurements of the atmospheric content of metallic ion and neutral species, Adv. Space Res. 33, 1481-1485, 2004.

[2] Axford, W. I., The formation and vertical motion of dense ionized layers in the ionosphere due to neutral wind shears, J. Geophys. Res., 68 (3), 769-779, 1963.

[3] Agabi E. Oshiorenoya, Plasma in the Ionosphere Ionization and Recombination. Space Physics 5P Umea Universitet Department of Physics Umea, Sweden July 2004.

[4] Alian, G. and Michel Petit, Ionospheric techniques and phenomena. Geophysics and Astrophysics Monographs, vol.13, pp. 171-174, 1978.

[5] Bishop,R.L., G.D. Earle,M. F. Larsen,C. M. Swenson,C. G. Carlson,P. A. Roddy,C. Fish,and T. W. Bullett, Sequential observations of the local neutral wind field structure associated with E region plasma layers. JOURNAL OF GEOPHYSICAL RESEARCH, VOL. 110, A04309, doi:10.1029/2004JA010686, 2005

[6] Bristow W.A. and B.J. Watkins, Numerical simulation of the formation of thin ionization layers at high latitudes. GEOPHYSICAL RESEARCH LETTERS, VOL. 18, NO.3 PAGES 404-407, MARCH 1991

[7] Carter L. N.,J. M. Forbes, Global transport and localized layering of metallic ions in the upper atmosphere. Ann. Geophysicae 17, 190-209 (1999)

[8] Chimonas, G., and W. I. Axford, Vertical movement of temperature zone sporadic E layers, J. Geophys. Res., 73, 111, 1968.

[9] Comfort R.H., Kinetic Description of Ionospheric Dynamics in the Three-Fluid Approximation. National Aeronautics and Space Administration Washington D. C. 20546, 1975

[10] Donahue T.M., A wind shear mechanism for producing sporadic-E by concentratng minor meteoric ions. SPACE RESEARCH COORDINATION CENTER NASA 1966

[11] Ferguson, E. E., Atmospheric metal ion chemistry, Radio Sci., 7 (3), 397-401, 1972.

[12] Keneshea T.J, M.A. MacLeod, Wind-Induced modification of E region ionization profile. JOURNAL OF THE ATMOSPHRIC SCIENCE VOLUME 23, SEP., 1970

[13] Larsen, M.F., A shear instablity seeding mechanism for quasiperiodic radar echoes, Jorn.Geo.Rea.. Vol. 105, No. A11, pages 24,931-24,940, Nov. 1,200

[14] MacDougall J.W., J.M.C. Plane, P.T. Jayachandran, Polar cap Sporadic-E: part 2, modeling Journal of Atmospheric and Solar-Terrestrial Physics 62 (2000) 11691176

[15] MacLeod M.A., sporadic-E theory. I. Collision-Geomagnetic Equilibrium. JOURNAL OF THE ATMOSPHRIC SCIENCE VOLUME 23, SEP. 1965

[16] MacLeod M.A., T.J. Keneshea, and R.S. Narcisi, Numerical Modelling of a metallic ion sporadic-E layer Radio Science, Volume 10, Number 3,pages 371-388, March 1975

[17] Mathews, J.D., Sopradic-E:current views and recent progress, Jour.Atmo. and solarterres. phys.,vol.60,pp. 413-435, 1998.

[18] Osterman, G. B., R. A. Heelis, and G. J. Bailey, Modeling the formation of intermediate layers at Arecibo latitudes, J. Geophys. Res., 99 (A6), 11,357-11,365, 1994.

[19] Roddy P. A.,Spatial and Temporal Structuring of Nighttime Intermediate Layers Above Wallops Island. Phd Thesis, University of Texas at Dallas, 2005

[20] Roddy P.A.,G. D. Earle, C. M. Swenson, C. G. Carlson, and T. W. Bullett, Relative concentrations of molecular and metallic ions in midlatitude intermediate and sporadic-E layers. GEOPHYSICAL RESEARCH LETTERS, VOL. 31, L19807, doi:10.1029/2004GL020604, 2004

[21] S.M.Radicella, Lecture notes on The quite and disturbed ionosphere. Areonomy and radiogarphy labratory, 2000 ICTP.

[22] Shalimov S. and C. Haldoupis, E-region wind-driven electrical coupling of patchy sporadic-E and spread-F at midlatitude. Annales Geophysicae, 23, 20952105, 2005 SRef-ID: 1432-0576/ag/2005-23-2095 European Geosciences Union 2005

[23] Smith L.G., Investigation of the influnce of winds in The lower ionosphere. NATIONALA AERONAUTICS AND SPACE ADMINISTRATION WASHINGTON 25, D. C. AUGUST 1963.

[24] Smith L.G., J.F. Bedinger, G.T. Best, E. Constantinides, Measurment of upper atospheric ionization and winds with a combined payload. NATIONALA AERONAUTICS AND SPACE ADMINISTRATION WASHINGTON 25, D. C. JUNE 1967.

[25] Smith L.G. and K.L. Miller, Sporadic-E layers and unstabel wind shears. Journal of Atmospheric and Terrestrial Physics, Vol. 42, pp. 45-50, 1979

[26] Wakabayashi T. and T. Ono, Multi-layer structure of mid-latitude sporadic-E observed during the SEEK-2 campaign. Annales Geophysicae, 23, 23472355, 2005 SRef-ID: 1432-0576/ag/2005-23-2347 European Geosciences Union 2005

[27] Whitehead J.D. The formation of a sporadic-E layer from vertical gradient in horizontal wind. Ionospheric sporadic-E layer, electromagnetism momograph. 1974

[28] Yokoyama T., M. Yamamoto, S. Fukao, T. Takahashi, and M. Tanaka, Numerical simulation of mid-latitude ionospheric E-region based on SEEK and SEEK-2 observations. Annales Geophysicae, 23, 23772384, 2005 SRef-ID: 1432-0576/ag/2005-23-2377 European Geosciences Union 2005

[29] Zamlutti, C.J, On the basic trends of the upper atmosphere modelling-a review, Revista brasileira de geofisica, vol.16n.2-3 Sao Paulo july/nov. 1998.

[30] Zamlutti, C.J The formal equations of the low latitude lower ionosphere and their applications Instituto Nacional de Pesquisas Espaciais - INPE, C.P. 515, 12245-970 São José dos Campos, SP, Brazil.

# DECLARATION

I declare that the thesis is my original work and has not been presented for a degree in any other university, and that all sources of materials have been duly acknowledged.

Name: Kibrom Bayru

Signature: _____

Date: _____

This thesis has been submitted for the examination with my approval as this thesis advisor.

Name: Dr. Baylie Damtie

Signature: _____

Date: _____